Attribution of sea ice model biases to specific model errors enabled by new induced surface flux framework

Alex West[1], Mat Collins[2], Ed Blockley[1], Jeff Ridley[1], Alejandro Bodas-Salcedo[1]

[1]Met Office Hadley Centre, FitzRoy Road, Exeter, EX1 3PB
[2]Centre for Engineering, Mathematics and Physical Sciences, University of Exeter, Exeter, EX4 4SB, UK

Correspondence to: Alex E. West (alex.west@metoffice.gov.uk)

Abstract. A new framework is presented for analysing the proximate causes of model sea ice biases, demonstrated with the CMIP5 model HadGEM2-ES. In this framework the sea ice volume is treated as a consequence of the integrated surface energy balance. A system of simple models allows the local dependence of the surface flux, as a function of time and space, on specific model variables (ice area, ice thickness, surface melt onset and downwelling longwave and shortwave radiation) to be described. When these are combined with reference datasets of the variable in question, it is possible to estimate the surface flux bias induced by the model bias in that variable.'. The method allows quantification of the role played by the surface albedo and ice thickness-growth feedbacks in causing anomalous sea ice melt and growth to the role played by other forcings which can be viewed as external to the sea ice state on short timescales. It shows biases in the HadGEM2-ES sea ice volume simulation to be due to a bias in spring surface melt onset date, partly countered by a bias in winter downwelling longwave radiation. The framework is applicable in principle to any model and has the potential to greatly improve understanding of the reasons for ensemble spread in modelled sea ice state.

1. Introduction

The Arctic sea ice cover has witnessed rapid change during the past 30 years, most notably with a decline in September extent of 1.05 x 10^6 km^2 / decade from 1986 to 2015 (HadISST1.2, Rayner et al 2003). In association with the changes in extent, evidence of declining Arctic sea ice thickness has been observed from submarine and satellite data (Rothrock et al, 2008, Lindsay and Schweiger, 2015). Arctic sea ice is also thought to have become younger on average as reserves of older ice have been lost (Maslanik et al, 2011), the onset of summer melt has been observed to become earlier in the year (Markus et al, 2009) and the onset of winter freezing has been observed to become later (Stammerjohn et al, 2012).

The changes have focussed much interest on model projections of Arctic sea ice, the loss of which influences the climate directly through increased absorption of shortwave (SW) radiation during summer and through greater release of heat from the ocean to the atmosphere during winter (Stroeve et al, 2012b). However, substantial spread remains in model simulations of present-day Arctic sea ice, and of the long-term rate of decline under climate change (Stroeve et al, 2012a). The causes of this spread are at present poorly understood, resulting in considerable uncertainty in future projections of Arctic sea ice.

Evaluating sea ice extent or volume with respect to reference datasets shows that some models clearly reproduce present-day sea ice state more accurately than others (e.g. Wang and Overland, 2012; Massonet et al, 2012; Shu et al, 2015). However, an accurate simulation of sea ice extent and volume under the present-day climate does

not necessarily imply an accurate future projection of sea ice change, as a correct simulation can be obtained by accident due to cancelling model errors, or internal variability. Sea ice extent in particular is known to be a very unsuitable metric for diagnosing model performance due to its high internal variability (Notz, 2015; Swart et al, 2015). Hence there is a need to better understand the drivers which lead a model to simulate a given Arctic sea ice state.

Ice volume is, to first order, proportional to the heat required to melt the ice, and therefore acts to integrate the surface and basal energy balance. Basal melting in the interior ice pack has been shown to derive in the main from direct solar heating of the ocean (e.g Maykut and McPhee, 1995), while basal freezing derives principally from conduction of energy upward through the ice (Perovich and Elder, 2002); this implies that the surface energy balance (SEB) contains the principal sources and sinks of energy for the sea ice on an Arctic-wide scale. However, a complex two-way relationship exists between sea ice thickness and surface energy balance, via the surface temperature and surface albedo, giving rise to the thickness-growth feedback (Bitz and Roe, 2004) and the surface albedo feedback (Bitz, 2008), both of which exert first-order control on the sea ice state. Hence many components of the SEB cannot be viewed as independent of the sea ice state in any meaningful sense.

This study, which presents a new framework to investigate the causes of modelled sea ice biases, is motivated by a desire to separate, to first order, many external drivers of the SEB (and hence the sea ice state) from the thickness-growth and albedo feedbacks, and thereby better understand the processes that result in a particular modelled sea ice state being simulated. The analysis uses as a case study the four members of the historical ensemble of the coupled model HadGEM2-ES, a member of the CMIP5 historical ensemblewhich simulates anomalously low annual minimum ice extent, and which simulates an ice volume which is both too low in the annual mean and too amplified in the seasonal cycle, a similar behaviour to that identified by Shu et al (2015) in the CMIP5 ensemble mean.

In the framework presented, the total surface flux is expressed in terms of key Arctic climate variables as functions of space and time using two simple models, for the freezing and melting seasons respectively, which are shown to capture well the large-scale spatial and seasonal variation of the surface flux. With the use of the simple models, the local dependence of modelled surface flux on key variables can be described. Hence, using reference datasets for the climate variables, the model bias in surface flux induced by each climate variable can be estimated. In this way, biases in ice growth and melt over the course of the year are attributed via the surface flux to biases in specific model quantities. The method allows the contributions to model biases in ice growth and melt caused by the sea ice albedo feedback, the ice thickness-growth feedback, and various external factors, to be separately quantified. In this way it can be seen how model biases in the external drivers are able to produce a particular sea ice state, offering a valuable tool for setting sea ice state biases in context, and for understanding spread in sea ice simulation within multimodel ensembles.

In Section 2, the HadGEM2-ES model and the observational datasets used are described in turn. In Section 3 the sea ice and surface radiation simulations of HadGEM2-ES are evaluated. In Section 4, the induced surface flux method is introduced, and in Section 5 the induced surface flux analysis is applied to HadGEM2-ES, allowing quantification of the role played by biases in specific Arctic climate variables in causing anomalous ice growth and melt. In Section 6 the implications of the results are discussed, in particular the mechanisms by which the

identified external drivers determine the modelled sea ice state, and the likely drivers behind the corresponding model biases. Conclusions are presented in Section 7.

2. Model and observational data

2.1 The HadGEM2-ES model

HadGEM2-ES is a coupled climate model employing additional components to simulate terrestrial and oceanic ecosystems, and tropospheric chemistry (Collins et al, 2011). It is part of the 'HadGEM2' family, a collection of models that all use the HadGEM2-AO coupled atmosphere-ocean system. HadGEM2-AO is developed from HadGEM1 (Johns et al, 2006), a coupled atmosphere-ocean model whose sea ice extent simulation was recognised as being among the closest to observations out of the CMIP3 ensemble models (Wang and Overland, 2009). While the atmospheric and ocean components of HadGEM2-ES contain a large number of improvements relative to HadGEM1, many of these targeted at improving simulations of tropical weather, the sea ice component is very similar to that of HadGEM1 except for three minor modifications (Martin et al, 2011, table A4).

A fundamental feature of the sea ice component of HadGEM2-ES, which is important for the analysis described in Section 4 below, is that it includes a sub gridscale sea ice thickness distribution (Thorndike et al, 1975). In this formulation, ice in each grid cell is separated into five thickness categories with boundaries at 0, 0.6m, 1.4m, 2.4m, 3.6m and 20m, each with its own area, thermodynamics and surface exchange calculations. It also includes elastic-viscous-plastic sea ice dynamics (Hunke and Dukowicz, 1997) and incremental remapping (Lipscomb and Hunke, 2004). The thermodynamic component is a zero-layer model, with no heat capacity, described in the appendix of Semtner (1976). The insulating effect of snow is modelled by means of a single layer with conductivity 0.33Wm-1K-1, also with no heat capacity (although sensible heat storage is parameterised in the top 10cm of the snow-ice column during surface exchange calculations, to aid stability). Most processes are calculated in the ocean model, but the surface energy balance (SEB) calculations are carried out in the atmosphere model, which passes top melting flux and conductive heat flux to the ocean model as forcing for the remaining components. A more complete description of the sea ice component can be found in McLaren et al (2006).

This study uses the four ensemble members of the CMIP5 historical experiment of HadGEM2-ES, forced with observed solar, volcanic and anthropogenic forcing from 1860 to 2005. The period 1980-1999 is chosen for the model evaluation, as a period which predates much of the recent rapid Arctic sea ice loss and is hence at least partially independent of the period normally used to evaluate sea ice trends. It has the added advantage of being recent enough to allow the use of a reasonable range of observational data. All analysis is carried out with data restricted to the Arctic Ocean region, shown in Figure 1.

2.2 Observational data

Uncertainty in observed variables tends to be higher in the Arctic than in many other parts of the world. There are severe practical difficulties with collecting in situ data on a large scale over regions of ice-covered ocean.

While satellites have in many cases been able to produce Arctic-wide measurements of some characteristics, most notably sea ice concentration, the relative lack of in situ observations against which these can be calibrated means knowledge of the observational biases is limited. Reanalysis data over the Arctic is also more subject to the reanalysis model errors than in other regions, due to errors in atmospheric forcing, and the existence of fewer direct observations available for assimilation (Lindsay et al, 2014). The approach of this study is to use a wide range of observational data to evaluate modelled sea ice state and surface radiative fluxes, and to use as reference datasets for the induced surface flux framework, using the small number of in situ validation studies to set results in context as far as possible.

To evaluate modelled sea ice fraction, we use the HadISST1.2 dataset (Rayner et al, 2003), derived from passive microwave observations. To evaluate modelled sea ice thickness Arctic-wide, we use the ice-ocean model PIOMAS (Schweiger et al, 2011), which is forced with the NCEP reanalysis and assimilates ice concentration data. Laxon et al (2013) and Wang et al (2016) found PIOMAS to estimate anomalously low winter ice thicknesses compared to satellite observations in some years. In particular, Wang et al (2016) found PIOMAS to have a mean bias of -0.31m relative to observations from the ICESat (Ice, Cloud and land Elevation Satellite) laser sensor. To set the PIOMAS comparison in context, we use two additional datasets to evaluate the model over smaller regions; measurements from radar altimetry aboard the ERS satellites from 1993-2000 (Laxon et al, 2003), limited to latitudes below 82°N; and estimates compiled by Rothrock et al (2008), derived from a multiple regression of submarine transects over the Central Arctic Ocean from 1975-2000, constrained to be seasonally symmetric.

To evaluate modelled surface radiative fluxes across the whole Arctic Ocean, three datasets are used. Firstly, we use the CERES-EBAF (Clouds and Earth's Radiant Energy Systems – Energy Balanced And Filled) Ed2.7 dataset (Loeb et al, 2009), based on direct measurements of top-of-atmosphere radiances from EOS sensors aboard NASA satellites, available from 2000 – present. Secondly, we use the ISCCP-FD (International Satellite Cloud Climatology Project FD-series) product (Zhang et al, 2004). Lastly, we use the ERA-Interim (ERAI) atmospheric reanalysis dataset, which provides gridded surface flux data from 1979-present using a reanalysis system driven by the ECMWF (European Centre for Medium-range Weather Forcecasts) IFS forecast model and the 4D-Var data assimilation system (Dee et al, 2011).

In-situ validation of these datasets in the Arctic has been limited, but Christensen et al (2016) found CERES to perform quite well relative to other products, albeit underestimating downwelling LW fluxes from November – February by 10-20 Wm^{-2} relative to in situ observations at Barrow (Alaska). Liu et al (2005) found ISCCP-FD to simulate SW radiative fluxes fairly accurately relative to observations from SHEBA, but to underestimate downwelling SW fluxes in spring by over 30 Wm^{-2}, also overestimating downwelling LW fluxes in winter by around 40 Wm^{-2} . Finally, Lindsay et al (2014) identified ERAI as producing a relatively accurate simulation of surface fluxes compared to in situ observations at Barrow (Alaska) and Ny-Ålesund (Svalbard), although tending to underestimate downwelling SW fluxes in the spring by up to 20 Wm^{-2} and overestimate downwelling LW fluxes in the winter by around 15 Wm^{-2}.

In addition to the datasets above, in section 4 we make use of satellite estimates of date of melt onset over sea ice (Anderson et al, 2012), also derived from passive microwave sensors; and in section 5, the CERES-SYN

dataset (Rutan et al, 2015), similar to CERES-EBAF but available at higher temporal resolution, is used to examine modelled surface radiation evolution during May in more detail.

3. Evaluating sea ice and surface radiation in HadGEM2-ES

From 1980-1999, the four members of the HadGEM2-ES historically-forced ensemble simulate a mean September sea ice extent of 5.78 x 10^6 km^2, with ensemble standard deviation of 0.24 x 10^6 km^2. By comparison, the mean observed September sea ice extent over this period was 6.88 x 10^6 km^2 according to the HadISST1.2 dataset. Over the reference period, therefore, modelled September sea ice extent is systematically lower than that observed (Figure 2a).

Mean ice thickness is consistently lower than that estimated by PIOMAS for the Arctic Ocean region (Figure 2b), with the highest biases of -0.4m occurring in October, close to the minimum of the annual cycle, and a near-zero bias in May, close to the maximum. Modelled ice thickness is also biased low relative to the ERS satellite measurements (Figure 2c), with thickness biases ranging from -0.57m in November to -0.16m in April, and relative to the submarine data (Figure 2d), with thickness biases ranging from -1.5m in August to -0.8m in January and May. Hence it is very likely that ice thickness in HadGEM2-ES is biased low in the annual mean, with biases tending to be higher when ice thickness is lower. In other words, the ice thickness annual cycle of HadGEM2-ES is likely to be too amplified, with both anomalously high ice melt during the summer and ice growth during the winter.

Maps of the ice thickness bias in April and October (Figure 2b-d) show agreement that the low ice thickness bias is smaller on the Pacific side of the Arctic than on the Atlantic side of the Arctic, becoming very small or even positive in the Beaufort Sea. There is also striking agreement in the spatial pattern of the amplification bias of the seasonal cycle, as diagnosed by April-October ice thickness difference (Figure 3). All three ice thickness datasets show the HadGEM2-ES ice thickness seasonal cycle to be too amplified across much of the Arctic, by up to 1m in the Siberian shelf seas; in addition, all show that in the Beaufort Sea, the amplification is nonexistent or even negative. There is clear association between areas where modelled annual mean ice thickness is biased low, and areas where the modelled seasonal cycle is overamplified, and vice versa.

In the following discussion of radiative fluxes, the convention is that positive numbers denote a downwards flux. Fluxes of downwelling SW radiation are higher in HadGEM2-ES than in all observational estimates during the spring (Figure 4a-c), with May biases of 22, 43 and 53 Wm^{-2} relative to CERES, ERAI, and ISCCP-FD respectively. We note that as ERAI and ISCCP-FD have been found to underestimate downwelling SW during spring at specific locations, the true model bias is perhaps more likely to lie towards the lower end of these estimates. During the summer, upwelling SW radiation is consistently lower in magnitude than in HadGEM2-ES, with June biases of 16, 37 and 44 Wm^{-2} with respect to ERAI, CERES and ISCCP-FD respectively (a positive bias in an upward flux demonstrates that the model is too low in magnitude). There is no consistent signal for a low bias in downwelling SW during the summer, suggesting a model surface albedo bias. The effect is that modelled net downward SW flux is too large with respect to all observational datasets in May and June, and with respect to some in July and August. Relative to CERES, the May downwelling SW bias displays no

clear spatial differentiation over the Arctic Ocean (Figure 4a), but the June upwelling SW bias, and hence the net SW bias, tend to be somewhat higher in magnitude towards the central Arctic (Figure 4b-c).

Fluxes of longwave (LW) radiation are lower in magnitude in HadGEM2-ES throughout the winter than in all observational datasets (Figure 4d-f). For downwelling LW, the mean model biases from December-April are -16, -22 and -40 Wm^{-2} for ERAI, CERES and ISCCP-FD respectively; for upwelling LW, the biases are 11, 16 and 18 Wm^{-2} for CERES, ERAI and ISCCP respectively. Because the downwelling LW biases vary more than the upwelling LW biases, there is uncertainty in inferring a model bias in net downwelling LW; ISCCP suggests a large model bias of -22 Wm^{-2}, CERES a smaller bias of -11 Wm^{-2}, while ERAI suggests a biasof only 1 Wm^{-2}. As in situ studies have shown both underestimation (by CERES) and overestimation (by ERAI and ISCCP-FD) of downwelling LW in winter, there is no clear indication as to where the true model bias in this quantity may lie. Maps of the downwelling and net down LW bias relative to CERES in February (Figure 4d,f) show the bias tends to be somewhat higher towards the North American side of the Arctic, and lower on the Siberian side.

In summary, there is evidence of a low bias in net downward LW during the winter, and a high bias in net downward SW during the summer, each of order of magnitude ~10 Wm^{-2}. This is consistent with surface radiation fluxes being the likely first-order cause of the amplified sea ice thickness seasonal cycle. In the next section we describe the process by which surface radiation biases can be attributed to particular model processes by calculating induced surface flux biases.

4. Calculating induced surface flux bias: Methods

In this section, and throughout the rest of the paper, a difference between a model simulation of a particular variable, and any reference dataset for that variable, is referred to as a 'bias'. In a similar way, the difference in model surface flux judged to arise from the difference in a particular variable relative to a reference dataset is referred to as an 'induced surface flux bias'. Attention is drawn to the fact that, due to observational inaccuracy, true model bias relative to the real world may be somewhat different from the biases described in this way.

Due to the latent heat of sea ice being an order of magnitude greater than the sensible heat required to raise the ice to the melting temperature, ice volume is very nearly proportional to the heat required to melt the ice. Ice volume therefore acts to integrate the surface and basal energy balance, and is largely determined by the fluxes at these interfaces. Across much of the Arctic the sea ice is insulated from the main source of heat energy from beneath, the warm Atlantic water layer, by fresh water derived mainly from river runoff (e.g. Serreze et al, 2006; Stroeve et al, 2012b). Because of this, in the Arctic Ocean interior direct solar heating of the ocean is likely to be an order of magnitude higher in accounting for basal melting of the sea ice, as observed by Maykut and McPhee, 1995, McPhee et al, 2003 and Perovich et al, 2008, and modelled by Steele et al (2010) and Bitz et al (2005). In particular, it has been found that in HadGEM2-ES oceanic heat convergence is of negligible importance to the sea ice heat budget (Keen et al, 2018). Hence the surface energy balance in the Arctic Ocean is of primary importance in controlling the evolution of sea ice volume.

We use a system of well-understood simple models, similar to those used in Thorndike (1992), to estimate, for each model grid cell, and month within the period, the rate at which the surface flux would be expected to change with a particular model variable. For each model grid cell and month, we construct a function $F_{sfc} \approx g_{x,t}(v_1,...,v_n)$, F_{sfc} being surface flux, where the v_i are climate variables that affect the surface flux on timescales shorter than that on which they affect each other, and can therefore be said to be independent for the purposes of this analysis. In this way, at each model grid cell and month the rate at which the surface flux depends on variable v_i can be approximated by $\partial g_{x,t}/\partial v_i$. Given a reference dataset for variable v_i, it then becomes possible to estimate, for each point in time and space, the surface flux bias induced by the bias in v_i as $\partial g_{x,t}/\partial v_i \left(v_{i,x,t}^{MODEL} - v_{i,x,t}^{REFERENCE}\right)$. The chief advantage of this method is that the resulting fields of induced surface flux bias can then be averaged in time or space to determine the large-scale effects of particular model biases, effectively bypassing nonlinearities in surface flux dependence.

The functions $g_{x,t}$ are constructed as follows. Firstly, a model grid cell in a particular month is classified as freezing or melting depending upon whether the monthly mean surface temperature is greater or lower than -2°C. If the grid cell is classified as freezing, the surface flux is approximated as

$$F_{sfc} \approx g_{x,t}^{w} = a_{ice}\left(F_{atmos-ice} + BT_{ocn}\right)\sum_{cat}\gamma_{ice-REF}^{cat}\left(1 - BR_{ice}^{cat}\right)^{-1} + \left(1 - a_{ice}\right)F_{atmos-ocean} \qquad (1)$$

Here $F_{atmos-ice} = F_{LW\downarrow} - \varepsilon_{ice}\sigma T_{sfc-REF}^4 + F_{sens-ice} + \left(1-\alpha_{ice}\right)F_{SW\downarrow}$, where a_{ice} is ice area, $F_{LW\downarrow}$, $F_{SW\downarrow}$ and $F_{sens-ice}$ downwelling longwave, shortwave and sensible heat flux respectively, the latter evaluated over only the ice-covered portion of the grid cell, ε_{ice} ice emissivity, $\sigma = 5.67\times10^{-8} Wm^{-2}K^{-4}$ the Stefan-Boltzmann constant, $T_{sfc-REF}$ is monthly mean surface temperature and α_{ice} is mean surface albedo over ice. $F_{atmos-ocean} = F_{LW\downarrow} - \varepsilon_{ocn}\sigma T_{ocn}^4 + F_{sens-ocn} + F_{lat-ocn} + \left(1-\alpha_{ocn}\right)F_{SW\downarrow}$, where ε_{ocn} is ocean surface emissivity, T_{ocn} ocean surface temperature (assumed to be -1.8°C), and $F_{sens-ocn}$ and $F_{lat-ocn}$ sensible and latent heat flux respectively over the ice-free portions of the grid cell. $B = 4\varepsilon_{ice}\sigma T_{sfc-REF}^3$ approximates the local rate of dependence of surface flux on surface temperature, T_b is ice base temperature, γ_{REF}^{cat} is the area of ice in ice thickness category *cat* as a fraction of total ice area, where *cat* ranges from 1 to 5, and $R_{ice}^{cat} = \frac{h_{ice}^{cat}}{k_I} + \frac{h_{snow}}{k_s}$ is the thermal insulance of the snow-ice column in category *cat,* where *cat* ranges from 1 to 5, k_I and k_s being ice and snow conductivity respectively, h_{ice}^{cat} and h_{snow} local ice and snow thickness.

If the grid cell is classified as melting, the surface flux is approximated as

$$F_{sfc} = g_{x,t}^{s} = F_{LW\downarrow} - \varepsilon_{ice}\sigma T_f^4 + F_{sens} + \left(a_{ice}\alpha_{ice} + \left(1-a_{ice}\right)\alpha_{ocn}\right)F_{SW\downarrow} \qquad (2)$$

where $T_f = 0°C$.

The ice surface albedo α_{ice} is further expressed as

$$\alpha_{ice} = (\alpha_{melt\_ice} - \alpha_{sea}) + I_{snow}(\alpha_{melt\_snow} - \alpha_{melt\_ice}) + (1-\gamma_{melt})(1-I_{snow})(\alpha_{cold\_ice} - \alpha_{melt\_ice}) + (1-\gamma_{melt})I_{snow}(\alpha_{cold\_snow} - \alpha_{melt\_snow}) \quad (3)$$

Here $\alpha_{sea} = 0.06$, $\alpha_{melt\_ice} = 0.535$, $\alpha_{melt\_snow} = 0.65$, $\alpha_{cold\_ice} = 0.61$ and $\alpha_{cold\_snow} = 0.8$ denote the parameterised albedos of open water, melting ice, melting snow, cold ice and cold snow respectively, and γ_{melt} denotes melting surface fraction as a fraction of ice area, while I_{snow} is an indicator for the presence of snow that is set to 1 or 0 depending on whether monthly mean snow thickness exceeds 1mm.

The derivation of the formulae is briefly described. The surface flux is composed of four radiative fluxes (downwelling and upwelling SW and LW), two turbulent fluxes (sensible and latent) and of an additional flux due to snowfall (which affects the surface flux as it represents a transfer of negative latent heat, since snow lying on ice changes the enthalpy of the snow-ice system). Hence $F_{sfc} = (1-\alpha_{ice}F_{SW}) + F_{LW\downarrow} - \varepsilon_{ice}\sigma T_{sfc}^4 + F_{sens} + F_{lat} + F_{snowfall}$ is used as a starting point from which the derivation of (2) follows in the melting season, assuming a surface temperature of 0°C and neglecting the snowfall contribution. (3) is designed to mimic the calculation of ice albedo in HadGEM2-ES, which parameterises the effect of meltponds after Curry (2001), reducing albedo linearly as surface temperature rises from -1°C to 0°C. (1) is derived by considering separately the contributions to F_{sfc} from the area of the grid cell covered by each ice category (and by open water). For each ice category, the conductive flux through the ice is assumed to be uniform; the dependence of F_{sfc} on surface temperature is then linearised, using monthly mean surface temperature at each grid point, $T_{sfc-REF}$, as a reference about which to take the linearization. By setting the conductive flux equal to F_{sfc} , the variable T_{sfc} is eliminated. Finally, the contributions to F_{sfc} are multiplied by category ice area and summed. In deriving (1), the contributions of the snowfall flux and of the latent heat flux over ice are neglected.

In this way, using equations (1)-(3), we construct the functions $g_{x,t}$, which depend on downwelling LW, downwelling SW, sensible heat flux, category ice thickness, category ice area (freezing cells), total ice area (melting cells), snow thickness, snow area and surface melt onset, variables which have the required property of tending to affect the surface flux on timescales shorter than that on which they affect each other. Hence at each point in space and time the rate of dependence of surface flux on each variable can be approximated by $\partial g_{x,t} / \partial v_i$. We describe for the case of three variables how this process can be used to estimate the surface flux bias induced by biases in that variable, firstly for the variable of melting surface fraction (for simplicity, we describe only the process over grid cells judged to be melting). Model daily surface temperature fields are used to judge, for each month of the year, the average melting surface fraction in each grid cell. The satellite-derived

observational estimates of surface melt onset described in Section 2.2 are used to produce a climatology of melting surface fraction for each month and grid cell, and this is subtracted to produce a model bias. This bias is then multiplied by the partial derivative of equation (2) with respect to melting surface fraction, $-F_{SW\downarrow}\left((1-I_{snow})(\alpha_{cold\_ice}-\alpha_{melt\_ice})+I_{snow}(\alpha_{cold\_snow}-\alpha_{melt\_snow})\right)$, evaluated with monthly mean fields of $F_{SW\downarrow}$ and I_{snow}, to produce a monthly mean field of surface flux bias induced by the model bias in melting surface fraction.

By a similar method, the effect of downwelling LW radiation on surface flux can be estimated, illustrated here using CERES as a reference dataset (in section 4 below the analysis is performed using multiple datasets) to produce fields of model bias in downwelling LW radiation. For freezing grid cells, these are then multiplied by $\sum_{cat} a_{cat}\left(1-BR_{ice}^{cat}\right)^{-1} \Big/ \sum_{cat} a_{cat}$, the partial derivative of (1) with respect to downwelling LW, to produce fields of surface flux bias induced by model bias in downwelling LW. For melting grid cells, the induced surface flux bias is equal to the downwelling LW bias, as the surface temperature does not change in response to the bias.

The most complex variable to analyse in this way is the ice thickness. Ice thickness strongly affects the surface flux in the freezing season; thicker ice is associated with less conduction, a colder surface temperature and a weaker negative surface flux, and hence reduced ice growth. However, it appears in equation (1) only implicitly, in the form of the individual category mean thicknesses h_I^{cat}. To use this equation to estimate the effect of ice thickness biases on surface flux, a method of estimating the way biases are distributed amongst thickness categories is needed. Given an estimated model bias in mean thickness $\overline{h}_{ice}^{'}$, it can be argued that the least arbitrary approach is to estimate the model bias in each thickness category to be $\overline{h}_{ice}^{'}$ also (i.e. the thickness distribution is uniformly shifted to higher, or lower values). However, this leads to unphysical results at the low end of the distribution; in the case of a negative bias, it implicitly assumes the creation of sea ice of negative thickness; in the case of a positive bias, it assumes that no sea ice of thicknesses between *0m* and $\overline{h}_{ice}^{'}$ *m* exists.

Hence we use a slightly modified approach. The model bias in the lowest thickness category is estimated to be $\overline{h}_{ice}^{'}/2$, equivalent to translating the top end of the category by $\overline{h}_{ice}^{'}$ but allowing the lower end to remain at 0. The model biases in the other four categories are then estimated to be $\overline{h}_{ice}^{'}\,\dfrac{a_{ice}-a_1/2}{a_{ice}-a_1}$, i.e. the translation is increased to ensure that the mean ice thickness bias remains correct. Following this, we iterate through the categories, identifying grid cells where the bias is such that a negative category sea ice thickness in the reference dataset is implied; in these cells, the bias is reduced such that the reference thickness in that category becomes 0, and the bias in the remaining categories is increased proportionally to ensure the mean sea ice thickness bias remains correct.

Hence we create, for each category, fields of sea ice thickness bias. These are multiplied by the partial derivative of equation (1) with respect to category ice thickness, $(A+BT_b)a_{cat}\left(1-BR_{cat}^{ice}\right)^{-2}\left(\sum_{cat}a_{cat}\right)^{-1}$, to create fields of induced surface flux bias for each category. These are then summed to obtain the total induced surface flux bias due to ice thickness bias.

The process of calculating induced surface flux bias is illustrated in Figure 5 for example months for these three variables. Figure 5a-c illustrates the melt onset analysis. Figure 5a shows the HadGEM2-ES bias in melting surface fraction for the month of June 1980, relative to the NSIDC climatology; the bias is generally positive, reflecting melt onset modelled earlier than observed during this month. Figure 5b shows the field of rate of change of surface flux with respect to melt onset occurrence (effectively downwelling SW multiplied by the difference in parameterised albedos); this tends to be higher in the Central Arctic, reflecting a greater tendency to clear skies here. Finally Figure 5c shows the product of these two fields, the modelled surface flux bias induced by the model bias in melt onset. This is also generally positive, by up to 25 Wm^{-2} in the central Arctic, reflecting the greater absorption of SW radiation induced by the early melt onset.

Figures 5d-f demonstrate the same process for the downwelling LW radiation in January 1980, using CERES as reference dataset. Modelled downwelling LW radiation is seen to be considerably lower in magnitude than that observed by CERES for the 2000-2013 period, by up to 30 Wm^{-2} in many parts of the Central Arctic (Figure 2d). The rate of change of surface flux with respect to downwelling LW is shown to be higher (closer to 1) in regions of thinner ice (Figure 2e). This has the result that the induced surface flux bias is greatly reduced relative to the downwelling LW bias in regions of thicker ice (Figure 2f), reflecting the lower efficiency of ice creation in regions of thicker ice; the bias is below $10Wm^{-2}$ over much of the Arctic, only approaching 20 Wm^{-2} in the Barents and Kara seas.

Figures 5g-i demonstrate the process of calculating surface flux bias induced by the bias in ice thickness in model category 1 (0-0.6m) for the month of January 1980, using PIOMAS as reference dataset. Modelled ice thickness tends to be thinner than estimated by PIOMAS over much of the Arctic for this month, except for an area on the Pacific side of the Arctic; as described above, the bias in category 1 is assumed to be half the total bias. Figure 5h shows the rate of change of surface flux with respect to category 1 ice thickness, which tends to be high in regions where category 1 ice covers higher fractions of the grid cell, generally near the ice edge.

5. Calculating induced surface flux bias: Results

Using the methods described in Section 4 we calculate surface flux biases induced by model biases in downwelling SW, downwelling LW, ice area, local ice thickness and surface melt occurrence. The resulting fields are averaged over the model period and over the Arctic Ocean region, to produce for each variable a seasonal cycle of surface flux bias induced by the bias in that variable. The induced surface flux (ISF) biases are displayed in Figure 6, together with total ISF bias, radiative flux biases estimated by the direct radiation evaluation relative to ISCCP-FD, CERES and ERAI, and also sea ice latent heat uptake biases implied by the

ice thickness biases relative to PIOMAS. The ISF biases are also shown in Table 1, using CERES as reference dataset for the radiative terms.

ISF biases tend to sum to negative values during the winter (indicating anomalous modelled energy loss and ice growth) and to positive values during the summer (indicating anomalous modelled energy gain and ice melt), consistent with the radiation and ice thickness evaluation. Major roles are identified for particular processes in certain months. Firstly, in June a bias in surface melt onset induces a surface flux bias of -13.6 Wm^{-2}, equivalent roughly to an extra 11cm of melt. This is associated with the meltpond parameterisation of HadGEM2-ES lowering the surface albedo at the end of May as the surface reaches the melting point, in contrast to SSMI observations which show surface melting to commence on average in mid to late June in the 1980-1999 period. Secondly, in August a bias in ice fraction induces a surface flux bias of 9.6 Wm^{-2}, equivalent to an extra 8cm of melt. This is associated with the overly fast retreat of sea ice in HadGEM2-ES, and the low extents in late summer, as noted in Section 3.

Thirdly, the large model biases in downwelling LW present throughout the freezing season induce substantial surface flux biases, ranging from -6.5 to -3.8 Wm^{-2} from October-March (the surface flux biases are considerably lower than the original downwelling LW biases because of the increasing inefficiency by which surface heat loss is converted to sea ice growth as ice thickens). Throughout this period, the total extra heat loss estimated by this process is roughly equivalent ice growth ranging from 20-33cm. Fourthly, the negative biases in ice thickness present at the end of summer also induce substantial surface flux biases which tend to decrease throughout the freezing season as the thickness biases decrease, with an induced surface flux bias of -8.3 Wm^{-2} in November reducing to -2.0 Wm^{-2} in March. This effect is roughly equivalent to an extra 24cm of ice growth. It is noted that while large ISF biases due to downwelling SW and LW are evident during summer, there is very large spread in these values between observational datasets, to the extent that the sign of the biases are uncertain. It is concluded that it is not possible to determine the net effect of downwelling radiative biases on surface flux during the summer with current observational data.

Internal variability in the ISF biases is measured by taking the standard deviation of the whole-Arctic ISF bias for each process and month across all 20 years in the model period, and all four ensemble members used. Variability is highest in the ice area term, reaching 4.0 Wm^{-2} in July. Variability reaches considerable size in some other terms in some months, for example 1.1 Wm-2 for surface melt onset in June, 1.9 Wm^{-2} for ice thickness in November, but is otherwise mainly under 1 Wm^{-2} in magnitude. In each case, therefore, the ISF biases noted above are persistent features of the model.

Residuals between the total ISF bias and the directly evaluated radiative flux biases (demonstrated using CERES as radiation reference dataset in Table 1) are comparable in magnitude to the differences between the three different evaluations of the radiative flux biases, indicating that observational uncertainty is likely to dominate uncertainty in the ISF biases themselves. For example, the residual between total ISF bias and net radiation bias varies from -15.4 Wm^{-2} in June to 8.1 Wm^{-2} in November, while the difference between net radiation bias as evaluated by CERES and ERAI respectively varies from -16.9 Wm^{-2} in July to -2.4 Wm^{-2} in September. As discussed in Section 3 above, evidence from in situ validation studies is inconclusive as to the true size of the modelled downwelling LW bias, and hence as to the magnitude of the surface flux bias induced by downwelling

LW. On the other hand, the evidence of PIOMAS underestimating winter sea ice thickness suggests that the magnitude of this bias, and the assosicated ISF bias, may be underestimated. It is also noted that there is a high uncertainty of the order ±10 Wm^{-2} in the ice area contribution during the winter. This is because the rate of dependence of surface flux on ice area is very high in freezing grid cells (generally 100-200 Wm^{-2}) due to the large differences between turbulent fluxes over sea ice and open water.

In Appendix A potential errors in the ISF analysis are discussed and are found to be quite small in magnitude relative to the difference between observational datasets. Firstly, due to sub-monthly variation in the component variables, the winter downwelling LW component may be underestimated in magnitude by around 0.6 Wm^{-2} on average, and the ice area component in August may be overestimated by around 1.6Wm^{-2}. Secondly, due to a separate effect by which the ISF biases do not exactly sum to the total surface flux bias, the total bias in October is likely to be overestimated in magnitude by 3.6 Wm^{-2}. Thirdly, due to nonlinearities in the surface flux dependence on ice thickness, the ice thickness component is overestimated in magnitude by 0.7 Wm^{-2} on average from October-April, with a maximum overestimation in November of 1.9 Wm^{-2}. We note that it is possible that in some months the sum of the ISF biases may be a truer representation of the actual surface flux bias than any of the individual evaluations, as the method combines observational estimates with physical relationships between the various flux components. For example, in the satellite datasets observational errors in the different components are not constrained to correlate in a physically realistic sense.

The most obvious discrepancy between the total ISF bias and the net radiation bias occurs in July, when the sum of the induced surface flux biases is small and of indeterminate sign, while a large positive bias is implied by the sea ice thickness and surface radiation simulations. This may be due to the 'missing process' of surface albedo bias due to the presence of snow on sea ice. Early surface melt onset, and sea ice fraction loss, as modelled by HadGEM2-ES, would be expected to be associated also with early loss of snow on sea ice, with an associated surface albedo bias, with this process reaching its maximum influence at a time between that of the surface melt onset (June) and that of the sea ice fraction loss (August). We note also that the direct effect of thinning ice on ice albedo could induce an additional flux bias relative to the real world, despite the fact that this effect is not modelled in HadGEM2-ES.

An annual mean total ISF bias of -3.6 (CERES) and -4.5 Wm^{-2} (ERAI) is present when the satellite datasets are used as reference (the annual mean total ISF bias for ERAI is -0.1 Wm^{-2}). It is noted that given a negligible contribution of oceanic heat convergence to the sea ice heat budget in HadGEM2-ES or in the real world, as is argued in Section 4, the annual mean surface flux bias would be expected to be substantially smaller than these figures, as a surface flux bias of -4.5 Wm^{-2} is equivalent to a relative thickening of the model sea ice cover by 9m over the 1980-1999 period. Analysis of potential sources of error in the ISF calculations in Appendix A does not produce evidence of a systematic bias that could explain these large annual mean negative biases, although the early-winter errors in the ice thickness component could explain a small portion (0.4 Wm^{-2}). Given the large discrepancy amongst observational datasets, therefore, it is likely that observational inaccuracy plays a significant part in introducing this annual mean bias.

Spatial patterns in the ISF biases are now discussed. Consistent with the pattern of net SW bias identified in section 3, the spatial pattern of surface flux bias induced by melt onset occurrence is characterised by a weak

maximum in the central Arctic, with values falling away towards the coast. A more sharply-defined pattern is produced by the ice fraction bias in August, with high values across the shelf seas and the Atlantic side of the Arctic falling to low or negative values in the Beaufort Sea; the pattern displayed by the ice thickness-induced bias in November is almost a mirror image. Finally, the surface flux bias induced by downwelling LW in February displays slightly higher values on the Siberian side of the Arctic than the North American side, the reverse pattern to that displayed by the downwelling LW itself in Figure 4d. The contrast is due to the role the effective ice thickness scale factor plays in determining the induced surface flux bias; thicker ice, such as that which tends to be found on the American side of the Arctic in both model and observations, tends to greatly reduce the flux bias. This represents the thickness-growth feedback, the reality that thicker ice will grow less quickly than thin ice under the same atmospheric conditions.

The spatial patterns of total ISF bias shows many similarities to total net radiation bias evaluated by CERES in most months of the year (Figure 7), notably a tendency in July and August for positive surface flux biases to be concentrated on the Atlantic side of the Arctic, and a tendency throughout the freezing season for negative surface flux biases to be least pronounced in the Beaufort Sea, where the ice thickness biases are likely to be lowest. We note that the spatial pattern of amplification of the ice thickness seasonal cycle displayed in Figure 3 is very similar, with amplification most pronounced near the Atlantic Ocean ice edge, and least pronounced in the Beaufort Sea.The surface flux biases produced by ice fraction biases in August, and ice thickness biases in November, provide reasons for the spatial variation in amplification of the ice thickness seasonal cycle seen in Figure 4, as well as the close resemblance of this pattern to the model biases in annual mean ice thickness. Ice which is thinner in the annual mean will tend to melt faster in summer, due to the net SW biases associated with greater creation of open water (the ice albedo feedback), and to freeze faster in winter, due to greater conduction of energy through the ice (the ice thickness-growth feedback).

6. Discussion

The calculation of the surface radiative flux biases induced by various key processes in the Arctic Ocean produces results qualitatively consistent with the surface radiation evaluation, and with the surface flux biases implied by the sea ice simulation. Melt onset occurrence and sea ice fraction biases tend to cause anomalous surface warming, and sea ice melt, during the summer, in the HadGEM2-ES historical simulation; downwelling LW and ice thickness biases tend to cause anomalous surface cooling, and hence sea ice growth, during the winter. It is helpful to divide the processes examined into feedbacks (surface flux biases induced by biases in the sea ice state itself) and forcings (those induced by downwelling radiative fluxes and melt onset occurrence). In this sense, a ‘forcing’ refers to a variable which is independent of the sea ice volume on short timescales, rather than being used in the traditional sense of a radiative forcing.

The surface flux bias induced by biases in ice fraction during the melting season can be identified with the effect of the surface albedo feedback on the sea ice state. This is because during the melting season the ice area affects the estimated surface flux only through the surface albedo, and the surface flux biases induced in this way cause associated biases in ice melt. On the other hand, the surface flux bias induced by biases in ice thickness during the freezing season can be identified with the effect of the thickness-growth feedback on the sea ice state. This is perhaps less obvious, as the ice thickness affects the estimated surface flux via the surface temperature and

upwelling LW radiation, while the thickness-growth feedback is usually understood to result from differences in conduction. However, the assumption of flux continuity at the surface in constructing the estimated surface flux means that the cooler surface temperatures, and shallower temperatures gradients occurring for thicker ice categories are manifestations of the same process. Slower ice growth at higher ice thicknesses has a manifestation in a smaller negative surface flux, and the surface temperature is the mechanism by which this is demonstrated. Hence the effect of the thickness-growth feedback is described by the ice thickness-induced component of the surface flux bias.

In this way, the ISF analysis allows the effect of the surface albedo and thickness-growth feedbacks on the sea ice state to be quantified, and compared to the effect of other drivers. Arctic-wide, the surface albedo feedback, diagnosed as the ice area-induced component of the surface flux bias, contributes an average of 5.2 Wm^{-2} to the surface flux bias over the summer months, equivalent to an extra 13cm of ice melt; this is very similar to the effect of the surface melt onset-induced component, which contributes an average of 5.3 Wm^{-2}, equivalent also to an extra 13cm of ice melt. In the freezing season, meanwhile, the thickness-growth feedback, diagnosed as the ice thickness-induced component of the surface flux bias, contributes an average of -4.4 Wm^{-2} to the surface flux bias from October-April, equivalent to an extra 26cm of ice freezing, while the downwelling LW-induced component (using CERES as reference dataset) contributes an average of -4.9 Wm^{-2}, equivalent to an extra 29cm of freezing over this period.

The biases of the HadGEM2-ES sea ice state can be understood by considering in turn the separate ISF components, their magnitudes, and the times of year when they are important..The anomalous summer sea ice melt is initiated by the early melt onset occurrence, and maintained by the surface albedo feedback, which acts preferentially in areas of thinner ice; the anomalous winter ice growth is maintained both by the thickness-growth feedback (occurring mainly in areas of thinner ice, of greater importance in early winter) and by the downwelling LW bias (more spatially uniform, in late winter). It is unclear that any significant role is played by the downwelling SWbias, as at the only time of year when the radiation datasets agree that this biasis of significant value (May), the induced surface flux biasis more than balanced by that induced by downwelling LW. However this may have a role in causing the later melt onset bias, as discussed below.

The means by which the external forcings – anomalous LW winter cooling, and early late spring melt onset – cause an amplified seasonal cycle in sea ice thickness are clear. It is also possible to understand how, in the absence of other forcings, these combine to create an annual mean sea ice thickness which is biased low, as seen in Section 3. The melt onset forcing, by inducing additional ice melting through its effect on the ice albedo, acts to greatly enhance subsequent sea ice melt through the surface albedo feedback. The downwelling LW, on the other hand, by inducing ice freezing, acts to attenuate subsequent sea ice freezing through the thickness-growth feedback. The effect is that surface flux biasesinduced by melt onset occurrence are enhanced, while those induced by downwelling LW are diminished.

Acting together, the ice thickness-growth feedback and surface albedo feedback create a strong association between lower ice thicknesses and amplified seasonal cycles, because ice which tends to be thinner will both grow faster during the winter, and melt faster during the summer. Hence the melt onset bias, acting alone, would induce a seasonal cycle of sea ice thickness lower in the annual mean, but also more amplified, than that

observed, because the surface albedo and thickness-growth feedbacks act to translate lower ice thicknesses into faster melt and growth. For similar reasons, the downwelling LW bias, acting alone, would induce a seasonal cycle of sea ice thickness higher in the annual mean, and also less amplified, than that observedThe bias seen in HadGEM2-ES is a result of the melt onset bias'winning out' over the downwelling LW, due to its occurring at a time of year when the intrinsic sea ice feedbacks render the ice far more sensitive to surface radiation. The anomalously low ice cover in September arises as a consequence of the low annual mean ice thickness, and in particular of the anomalously severe summer ice melt. The finding that the low annual mean ice thickness is driven by surface albedo biases is consistent with the finding by Holland et al (2010) that variance in mean sea ice volume in the CMIP3 ensemble was mostly explained by variation in summer absorbed SW radiation.

The feedbacks of the sea ice state explain the association between spatial patterns of annual mean ice thickness bias and ice thickness seasonal cycle amplification. However, the external forcings (melt onset and downwelling LW bias) cannot entirely explain the spatial patterns in the mean sea ice state biases, because on a regional scale effects of sea ice convergence, and hence dynamics, become more important. The annual mean ice thickness bias seen in HadGEM2-ES is associated with a thickness maximum on the Pacific side of the Arctic, at variance with observations which show a similar maximum on the Atlantic side. It was shown by Tsamados et al (2013) that such a bias could be reduced by introducing a more realistic sea ice rheology.

The study would be incomplete without a discussion of possible causes of the two external drivers identified by this analysis as causing sea ice model biases. Underestimation of wintertime downwelling LW fluxes in the Arctic is known to be a widespread model bias in the CMIP5 ensemble (e.g. Boeke and Taylor, 2016). Pithan et al (2014) showed that this bias was likely to be a result of insufficient liquid water content of clouds forming in subzero air masses, resulting in a failure to simulate a particular mode of Arctic winter climate over sea ice; the 'mild mode', characterised by mild surface temperatures and weak inversions, whose key diagnostic is observed to be a net LW flux of close to 0 Wm^{-2} (Stramler et al, 2011; Raddatz et al, 2015 amongst others). HadGEM2-ES was not one of the models assessed by Pithan et al (2014), but its winter climate simulation displays many of the characteristic biases displayed by these, notably a tendency to model very low cloud liquid water fractions during winter compared to MODIS observations (Figure 8a) and a failure to simulate the milder mode of Arctic winter climate as demonstrated in SHEBA observations, diagnosed by 6-hourly fluxes of net LW (Figure 8b). Here we conclude that a similar mechanism is likely to be at work in HadGEM2-ES, and that insufficient cloud liquid water is the principal driver of the anomalously low downwelling LW fluxes.

The causes of the early melt onset bias of HadGEM2-ES are harder to determine. For most of the spring, comparison of daily upwelling LW fields of HadGEM2-ES to CERES-SYN observations (not shown) shows the Arctic surface to be anomalously cold in the model, as during the winter. During May, however, upwelling LW values rise much more steeply in the model, and surface melt onset commences during mid-to-late May, far earlier than in the satellite observations. A possible cause of the overly rapid surface warming during May is the zero-layer thermodynamics approximation used by HadGEM2-ES, in which the ice heat capacity is ignored. Comparing fields of surface temperature in HadGEM2-ES between the beginning and the end of May shows a 'missing' ice sensible heat uptake flux of 10-30 Wm^{-2} over much of the central Arctic, which would in turn be associated with a reduction of flux into the upper ice surface of 5-15 Wm^{-2}. Examination of modelled and observed daily timeseries of downwelling LW and net SW fluxes in late May and early June suggests that a

surface flux reduction of this magnitude could delay surface melt by up to 2 weeks, a substantial part of the modelled melt onset bias seen.

Another cause of the rapid warming may be the increasing relative magnitude of the downwelling SW response to cloud biases as May progresses (compared to the downwelling LW response). Comparison of 5-daily means of HadGEM2-ES radiative fluxes during May to those from the CERES-SYN product (not shown) support this hypothesis; a modelled bias in downwelling SW grows quickly during early May, from ~ 0Wm^{-2} to ~ 30Wm^{-2}, while the modelled bias in downwelling LW remains roughly constant.

The ISF analysis as presented does not comprise an exhaustive list of processes affecting Arctic Ocean surface fluxes. The missing processes of the effects of snow fraction and ice thickness bias on the surface albedo have already been noted; the effect of snow thickness bias on winter conduction and surface temperature is another such process which cannot be included due to inadequate observations. Model biases in the turbulent fluxes may also be significant; while the process which is likely most important in determining these during the winter is captured (ice fraction in the freezing season), a more detailed treatment of turbulent fluxes would also examine the effect on these of the overlying atmospheric conditions. It is also noted that snowfall itself is a component of the surface flux which could in theory be evaluated directly given a sufficiently reliable observational reference.

Finally, it is noted that a complete treatment of model biases affecting the sea ice volume budget would also examine causes of bias in oceanic heat convergence. For the reasons discussed in Section 4 these are likely to be small in the Arctic Ocean interior in HadGEM2-ES and observations, but the model bias could nevertheless conceivably be of considerable size in the context of the surface flux biases shown in Figure 6. The total Arctic Ocean heat convergence modelled by HadGEM2-ES for the period 1980-1999 is 4.4 Wm^{-2}, although this figure shows high sensitivity to the location of the boundary in the Atlantic sector, suggesting that most of this heat is released close to the Atlantic ice edge. This figure is slightly higher than the 3 Wm^{-2} found by Serreze et al (2007) in their analysis of the Arctic Ocean heat budget, but is broadly consistent with observational estimates of oceanic heat transport through the Fram Strait (likely to be the major contributor to Arctic Ocean heat convergence) from 1997 to 2000 by Schauer et al, 2004. This suggests that errors in oceanic heat convergence are unlikely to contribute significantly to sea ice volume biases in HadGEM2-ES. However, for a hypothetical model which simulated greater oceanic heat convergence in the Arctic Ocean interior, the surface flux analysis presented here would fail to adequately describe the model bias in the sea ice volume budget.

7. Conclusions

HadGEM2-ES simulates a sea ice cover which is not extensive enough at annual minimum. Comparison to various ice thickness datasets shows that it also has too low an annual mean ice thickness, and that its ice thickness seasonal cycle is likely to be overamplified. Evidence of a positive net SW bias during the ice melt season, and a negative net LW bias during the ice freezing season is apparent from evaluations using multiple radiation datasets.

An evaluation of processes influencing surface radiation, combined with simple models to estimate their effect, produces results consistent with the evaluation of the sea ice state and surface radiation; processes tend to cause

anomalous ice melt during the melting season, and anomalous ice growth during the freezing season. Consequently model biases in sea ice growth and melt rate can be attributed in detail to different causes; in particular, the roles played by the sea ice albedo feedback, by the sea ice thickness-growth feedback, and by external forcings, can be quantified. The analysis reveals how the melt onset bias of HadGEM2-ES tends to make model ice thickness both low in the annual mean, and too amplified in the seasonal cycle, with the downwelling LW bias acting to mitigate both effects. The result is consistent with the prediction of DeWeaver et al (2008) that sea ice state is more sensitive to surface forcing during the ice melt season than during the ice freeze season. The analysis also suggests that through an indirect effect on surface albedo at a time when sea ice is particularly sensitive to surface radiation biases, the zero-layer approximation, which was until recently commonplace in coupled models, may be of first-order importance in the sea ice state bias of HadGEM2-ES.

A clear link has been demonstrated between the spatial pattern of biases in annual mean ice thickness, likely driven by ice dynamics, and that of biases in the April-October thickness. Where ice thickness is biased low in the annual mean, an enhanced seasonal cycle is apparent. This is due to the thickness-growth and ice albedo feedbacks, initiated by melt early melt onset and downwelling LW bias, both of which are spatially uniform.

Large observational uncertainties for snow cover and summer surface radiation limit the overall accuracy of the methodology presented here. The addition of freezing season snow thickness, and melt season snow fraction, would represent useful extensions to the analysis presented. An additional caveat regarding this analysis is that it does not consider factors influencing turbulent fluxes (with the exception of the ice area, but this contribution is subject to particularly high uncertainty). It also does not consider the influence of oceanic heat convergence on sea ice state; in HadGEM2-ES the latter is small (~10%), but might be more significant in other models.

In the case study presented here, the analysis provides mechanisms behind a model bias in sea ice simulation. However, the analysis could also be used to investigate a sea ice simulation that was ostensibly more consistent with observations, to determine whether or not the correct simulation was the consequence of model biases that cause opposite errors in the surface energy budget; a negative result would greatly increase confidence in the future projections of such a model. The analysis could be also used to investigate a whole model ensemble, to attribute spread in modelled sea ice state to spread in the underlying processes affecting the SEB, focussing attention on ways in which spread in modelled sea ice could be reduced. It is noteworthy that Shu et al (2015) found the CMIP5 ensemble mean Arctic sea ice volume to be biased low in the annual mean, and overamplified in the seasonal cycle, relative to PIOMAS (albeit over the entire Northern Hemisphere), suggesting that the behaviour exhibited by HadGEM2-ES may be quite common in this ensemble.

Finally, it is suggested that the ISF method, as well as being used to compare a model to observations, could also be used to understand the reasons for the biases of one model with respect to another. Such a comparison would avoid the issues of observational uncertainty discussed above, enabling the contributions of the different model variables to the surface flux biases to be evaluated more accurately.

Appendix A: Analysis of potential errors in ISF bias calculation

Due to observational uncertainty, it is difficult to directly evaluate the ISF bias calculations. Instead, we examine in turn the two principal sources of error in the method; firstly, error in correctly characterising the dependence of surface flux on a climate variable, and secondly, error in approximating the surface flux bias induced by this as the product of the surface flux dependence with the model bias in that variable.

To analyse the first source of error, we begin by comparing fields of the approximated surface flux $g_{x,t}$ to those of the real modelled surface flux F_{sfc}. The $g_{x,t}$ are found to capture well the large-scale seasonal and spatial variation in surface flux, but are prone to systematic errors which vary seasonally, indicated in Figure A1; firstly, a tendency to underestimate modelled negative surface flux in magnitude from October-April by 13% on average; secondly, a tendency to overestimate modelled positive surface flux from June-August by up to 10 Wm-2; thirdly, during May, a underestimation varying from 5-20 Wm-2.

Examining first the winter underestimation (demonstrated in Figure A1 a-c), it is found that for each model month the relationship between estimated and actual surface flux is strongly linear, with underestimation factors ranging from 6 ± 1% in December to 17 ± 2% in April. This suggests that the cause lies in systematic underestimation of the scale factor $\sum_{cat} \gamma_{ice-REF}^{cat} \left(1 - BR_{ice}^{cat}\right)^{-1}$. A possible cause is covariance in time between $\gamma_{ice-REF}^{cat}$ and R_{ice}^{cat} within each month, particularly in the first ice category; during the freezing season, occurrence of high fractions of ice in category 1, the thinnest category, would be expected to be associated with formation of new ice, and correspondingly lower mean thicknesses of ice in this category, lower values of R_{ice}^{cat} and higher values of $\left(1 - BR_{ice}^{cat}\right)^{-1}$. A calculation using daily values of $\gamma_{ice-REF}^{cat}$ ranging from 0.1 – 0.5, and daily values of h_I^{cat} ranging from 0.2 – 0.5m, predicts that this effect would in this case lead to an underestimation of 9% in the magnitude of the surface flux, sufficient to explain all of the underestimation in October, December and January, and most in November, February and March. This effect would produce a corresponding underestimation of the rate of dependence of surface flux on downwelling LW radiation and ice thickness throughout the freezing season. It was estimated that the downwelling LW component of the ISF bias is underestimated by 0.6 Wm^{-2} for the freezing season on average due to this effect.

Secondly, we examine the tendency to overestimate surface flux during the summer (Figure A1d-f), an effect that displays a spatially uniform bias rather than a spatially uniform ratio, ranging from 5-15 Wm^{-2} in July and August; the bias is smaller, and in the central Arctic negative, during June. A possible contributing factor to this bias is within-month covariance between ice area and downwelling SW; during July and August, both downwelling SW and surface albedo fall sharply, an effect that would tend cause the monthly mean surface flux to be overestimated. To estimate this effect, monthly trends in these variables were estimated by computing half the difference between modelled fields for the following and previous month. For July, an overestimation in surface flux of magnitude 5-15 Wm^{-2} was indeed predicted in the Siberian seas, as well as the southern Beaufort

and Chukchi Seas; however, in the central Arctic no overestimation was predicted, due to near-zero trends in ice area in the summer months. It is possible that some covariance between ice area and downwelling SW is nevertheless present in these regions, due to enhanced evaporation and cloud cover in regions of reduced ice fraction.

However, this effect would have no direct impact on the ISF biases because these are computed from monthly means of the model bias in one variable by the model mean in the other; hence, it is covariance between bias and mean that would induce inaccuracy in this case. By similarly approximating the trend in monthly mean model bias as half the difference between model bias in the adjacent months, the error in downwelling SW and ice area contributions were evaluated. Error in the downwelling SW term was found to be significant early in the summer, with an error of -2.7 Wm^{-2} in June; error in the ice area term was found to be significant later in the summer, with errors of -1.7 Wm^{-2} and -1.6 Wm^{-2} in July and August respectively. However, the August error is small relative to the total ISF bias identified.

Thirdly, we examine the reasons for the underestimation of surface flux in May (Figure A1g-i), a pattern unique to this month which is seen to be small in the central Arctic but to approach 20 Wm^{-2} at the Arctic Ocean coasts. A likely cause of this inaccuracy is the classification of grid cells as 'freezing' or 'melting' for entire months. During May, as has been seen, most model grid cells in fact cross from one category to the other; however, virtually all Arctic Ocean grid cells are classified as freezing for the month as a whole. The difference field between estimated 'freezing surface flux' and 'melting surface flux' is similar in magnitude and in spatial pattern to the underestimation field, being near-zero in the central Arctic but rising to 25 Wm^{-2} close to the Arctic Ocean coasts. It is concluded that the actual model mean surface flux is much higher than that estimated near the coast due to these grid cells experiencing melting conditions from relatively early in the month. Although this error is not directly relevant to the results of this paper, as no unequivocal ISF biases were identified for May, it would have the potential to lead to overestimation of the dependence of surface flux on ice thickness, and underestimation of dependence on all other variables, as the upwelling LW flux is unable to counteract changes in surface forcing once the surface has hit the melting point.

Having examined potential causes of error in estimating dependence of surface flux on individual variables, the validity of estimating ISF biases as the product of these with model variable biases is now discussed. Even if the dependence of monthly mean surface flux on variable v_i at a model grid cell is perfectly described by $\partial g_{x,t} / \partial v_i$, that dependence changes as the realisation varies from the model state to the real-world state. As a simplified example, a component of the surface flux, net SW, is equal to $F_{SW\downarrow}\left(1-\alpha_{sfc}\right)$, and induced surface flux biases due to model biases in $F_{SW\downarrow}$ and α_{sfc} would be calculated as $F'_{SW\downarrow}\left(1-\alpha_{sfc}^{\mathrm{mod}}\right)$ and $F_{SW\downarrow}^{\mathrm{mod}}\alpha'_{sfc}$ respectively. However, the sum of the two induced surface flux biases will not be exactly equal to the true surface flux bias, $F_{SW\downarrow}^{\mathrm{mod}}\left(1-\alpha_{sfc}^{\mathrm{mod}}\right)-F_{SW\downarrow}^{obs}\left(1-\alpha_{sfc}^{obs}\right)$, but will differ from it by $F'_{SW\downarrow}\alpha'_{sfc}$. This is due to the dependencies being evaluated on model states which are themselves biased.

This apparent problem can be resolved only by viewing the ISF method as a way not simply of estimating model biases due to a particular variable, but of characterising them, i.e. by accepting that the quantity that we are

trying to estimate is itself somewhat subjective. Instead of requiring the ISF method to be correct, it is required that it gives useful, physically realistic results. In the case given above, a sufficient condition is that $F'_{SW\downarrow}\alpha'_{sfc}$ is small relative to $F'_{SW\downarrow}\left(1-\alpha^{\mathrm{mod}}_{sfc}\right)$ and $F^{\mathrm{mod}}_{SW\downarrow}\alpha'_{sfc}$, i.e. that the model bias in both downwelling SW and in surface albedo is small relative to the absolute magnitudes of these variables.

More generally, the difference between the surface flux bias F'_{sfc} and the sum of the induced surface flux biases $\sum_i v'_i \partial g_{x,t}/v_i$ can be approximated by $\sum_{\substack{i,j \\ i\neq j}} v'_i v'_j \partial^2 g_{x,t}/\partial v_i \partial v_j$, a term that can be calculated relatively easily as many of the derivatives go to zero. Averaged over the Arctic Ocean this term was small in most months of the year, but of significant size in October (3.6 $\mathrm{Wm^{-2}}$), due to co-location of substantial negative biases in downwelling LW and category 1 ice thickness in this month, indicating that the true surface flux bias in this month may be substantially smaller (in absolute terms) than the -11.5 $\mathrm{Wm^{-2}}$ obtained from summing the ISF biases.

Finally, the induced surface flux calculation implicitly assumes a linear dependence of surface flux on each climate variable. However, this is not the case for the ice thickness, where higher-order derivatives do not go to zero, and in some regions of thinner ice actually diverge. It is possible to quantify the error introduced by the assumption of linearity by comparing the partial derivative $\left(A+BT_b\right)a_{cat}\left(1-BR^{ice}_{cat}\right)^{-2}\left(\sum_{cat} a_{cat}\right)^{-1}$ to the quantity $\left(A+BT_b\right)a_{cat}\left(1-BR^{ice}_{cat}\right)^{-1}\left(1-BR^{ice-REF}_{cat}\right)^{-1}\left(\sum_{cat} a_{cat}\right)^{-1}$, where $R^{ice-REF}_{cat}=h^{OBS}_I/k_I+h_S/k_S$, h^{OBS}_I being climatological ice thickness in the reference dataset, in this case PIOMAS, and all other terms defined as in Section 4. It can be shown that multiplying this quantity by the model bias produces the exact bias in estimated surface flux that is being approximated by $\partial g_{x,t}/\partial h_I\left(h^{MODEL}_I-h^{OBS}_I\right)$. Hence the bias in the ice thickness component induced by the nonlinearity can be calculated directly. It is found that the nonlinearity causes the ice thickness component to be overestimated in magnitude by 0.7 $\mathrm{Wm^{-2}}$ on average from October-April, with a maximum overestimation of 1.9 $\mathrm{Wm^{-2}}$ in November.

Code availability

The code used to create the fields of induced surface flux bias is written in Python and is provided as a supplement (directory 'ISF'). The code used to create Figures 1-8, as well as Figure A1, is also provided(directory 'Figures'). In addition, the routines used to estimate errors in the ISF analysis are provided (directory 'Analysis'). Finally, the code used to create Table 1 is provided (directory 'Tables'). A set of auxiliary routines used by most of the above are also provided (directory 'Library').. Most routines make use of the open source Iris library, and several make use of the open source Cartopy library.

Data availability

Monthly mean ice thickness, ice fraction, snow thickness and surface radiation, as well as daily surface temperature and surface radiation, for the first historical member of HadGEM2-ES, is available from the CMIP5 archive at https://cmip.llnl.gov/cmip5/data_portal.html.

NSIDC ice concentration and melt onset data can be downloaded at http://nsidc.org/data/NSIDC-0051 and http://nsidc.org/data/NSIDC-0105 respectively.

PIOMAS ice thickness data can be downloaded at http://psc.apl.uw.edu/research/projects/arctic-sea-ice-volume-anomaly/data/.

ERAI surface radiation data can be downloaded at http://apps.ecmwf.int/datasets/data/interim-full-daily/levtype=sfc/.

ISCCP-FD surface radiation data is available at https://isccp.giss.nasa.gov/projects/browse_fc.html.

CERES surface radiation data is available at https://climatedataguide.ucar.edu/climate-data/ceres-ebaf-clouds-and-earths-radiant-energy-systems-ceres-energy-balanced-and-filled.

Acknowledgements

This work was supported by the Joint UK BEIS/Defra Met Office Hadley Centre Climate Programme (GA01 101), and the European Union's Horizon 2020 Research & Innovation programme through grant agreement No. 727862 APPLICATE.

Thanks are due to Richard Wood and Ann Keen for helpful comments on multiple versions of this study.

References

Anderson, M., Bliss, A. and Drobot, S.: Snow Melt Onset Over Arctic Sea Ice from SMMR and SSM/I-SSMIS Brightness Temperatures, Version 3. Boulder, Colorado USA. NASA National Snow and Ice Data Center Distributed Active Archive Center. doi: http://dx.doi.org/10.5067/22NFZL42RMUO [accessed October 2015], 2001, updated 2012

Bitz, C. M. and Roe, G. H.: A Mechanism for the High Rate of Sea Ice Thinning in the Arctic Ocean, J. Clim., 17, 18, 3623–3632, doi: https://doi.org/10.1175/1520-0442(2004)017, 2004

Bitz, C. M., Holland, M. M., Hunke, E. C., and Moritz, R. M.: Maintenance of the Sea-Ice Edge, J. Clim., 18, 15, 2903–2921, doi: https://doi.org/10.1175/JCLI3428.1, 2005

Bitz, C. M.: Some Aspects of Uncertainty in Predicting Sea Ice Thinning, in Arctic Sea Ice Decline: Observations, Projections, Mechanisms, and Implications (eds E. T. DeWeaver, C. M. Bitz and L.-B. Tremblay), American Geophysical Union, Washington, D.C.. doi: 10.1029/180GM06, 2008

Boeke, R. C. and Taylor, P. C.: Evaluation of the Arctic surface radiation budget in CMIP5 models, J. Geophys. Res. Atmos., 121, 8525-8548, doi:10.1002/2016JD025099, 2016

Christensen, M. W., Behrangi, A., L'ecuyer, T. S., Wood, N. B., Lebsock, M. D. and Stephens, G. L.: Arctic Observation and Reanalysis Integrated System: A New Data Product for Validation and Climate Study, B. Am. Meteorol. Soc., 97, 6, 907–916, doi: https://doi.org/10.1175/BAMS-D-14-00273.1, 2016

Collins, W. J., Bellouin, N., Doutriaux-Boucher, M., Gedney, N., Halloran, P., Hinton, T., Hughes, J., Jones, D., Joshi, M., Liddicoat, S., Martin, G., O'Connor, F., Rae, J., Senior, C., Sitch, S., Totterdell, I., Wiltshire, A. and Woodward, S.: Development and evaluation of an Earth-System model – HadGEM2. Geosci. Model Dev., 4, 1051-1075. doi:10.5194/gmd-4-1051-2011, 2011

Dee, D. P, Uppala, S. M., Simmons, A. J., Berrisford, P., Poli, P., Kobayashi, S., Andrae, U., Balmaseda, M. A., Balsamo, G., Bauer, P., Bechtold, P., Beljaars, A. C. M., van de Berg, L., Bidlot, J., Bormann, N., Belsol, C., Dragani, R., Fuentes, M., Geer, A., J., Haimberger, L., Healy, S. B., Hersbach, H., Holm, E. V., Isaksen, L., Kållberg, P., Köhler, M., Matricardi, M., McNally, A. P., Monge-Sanz, B. M., Morcrette, J.-J., Park, B.-K., Peubey, C., de Rosnay, P., Tavolato, C., Thépaut, J.-N. and Vitart, F.: The ERA-Interim reanalysis: configuration and performance of the data assimilation system. Quarterly Journal of the RMS 137:553:597. doi: 10.1002/qj.828, 2011

DeWeaver, E. T., Hunke, E. C. and Holland, M. M.: Sensitivity of Arctic Sea Ice Thickness to Intermodel Variations in the Surface Energy Budget. AGU Geophysical Monograph 180: Arctic Sea Ice Decline: Observations, Projections, Mechanisms and Implications, 77-91. doi: 10.1029/180GM07, 2008

Gultepe, I., Isaac, G. A., Williams, A., Marcotte, D. and Strawbridge, K. B., Turbulent heat fluxes over leads and polynyas, and their effects on arctic clouds during FIRE.ACE: Aircraft observations for April 1998, Atmosphere-Ocean, 41:1, 15-34, DOI: 10.3137/ao.410102, 2003

Holland, M.M., Serreze, M.C. and Stroeve, J., The sea ice mass budget of the Arctic and its future change as simulated by coupled climate models, Clim Dyn (2010) 34: 185. doi:10.1007/s00382-008-0493-4

Hunke, E. C. and Dukowicz, J. K., An Elastic–Viscous–Plastic Model for Sea Ice Dynamics, J. Phys. Oceanogr., 27, 9, 1849–1867, doi: https://doi.org/10.1175/1520-0485(1997)027<1849:AEVPMF>2.0.CO;2, 1997.

Johns, T. C., Durman, C. F., Banks, H. T., Roberts, M. J., McLaren, A. J., Ridley, J. K., Senior, C. A., Williams, K. D., Jones, A., Rickard, G. J., Cusack, S., Ingram, W. J., Crucifix, M., Sexton, D. M. H., Joshi, M. M., Dong, B.-W., Spencer, H., Hill, R. S. R., Gregory, J. M., Keen, A. B., Pardaens, A. K., Lowe, J. A., Bodas-Salcedo, A., Stark, S. and Searl, Y.: The New Hadley Centre Climate Model (HadGEM1): Evaluation of Coupled Simulations. J Clim 19:1327-1353. doi: 10.1175/JCLI3712.1, 2006

Keen, A. B., Blockley, E., Investigating future changes in the volume budget of the Arctic sea ice in a coupled climate model, The Cryosphere, 12, 2855-2868, doi: 10.5194/tc-12-2855-2018, 2018.

Laxon, S., Peacock, N. and Smith, D.: High interannual variability of sea ice thickness in the Arctic region. Nature, 425, 947-950, doi:10.1038/nature02050, 2003

Laxon, S., Giles, K. A., Ridout, A., Wingham, D. J., Willatt, R., Cullen, R., Kwok, R., Schweiger, A., Zhang, J., Haas, C., Hendricks, S., Krishfield, R., Kurtz, N., Farrell, S. and Davidson, M.: Cryosat-2 estimates of Arctic sea ice thickness and volume. Geophys Res Lett 40:732-737. doi: 10.1002/grl.50193, 2013

Lindsay, R., Wensnahan, M., Schweiger, A. and Zhang, J.: Evaluation of Seven Difference Atmospheric Reanalysis Products in the Arctic, J. Clim., 27, 2588-2606, oi: 10.1175/JCLI-D-13-00014.1, 2013.

Lindsay, R. and Schweiger, A.: Arctic sea ice thickness loss determined using subsurface, aircraft, and satellite observations. The Cryosphere, 9, 269-283. doi: 10.5194/tc-9-269-2015, 2015

Lipscomb, W. H. and Hunke, E. C., Modeling Sea Ice Transport Using Incremental Remapping, Mon. Weather Rev., 132, 6, 1341–1354, doi: https://doi.org/10.1175/1520-0493(2004)132<1341:MSITUI>2.0.CO;2, 2004

Liu, J., J. A. Curry, Rossow, W. B., Key, J. R. and Wang, X.: Comparison of surface radiative flux data sets over the Arctic Ocean. J. Geophys. Res.: Oceans, 110, C2, doi: 10.1029/2004JC002381, 2005

Loeb, N. G., Wielicki, B. A., Doelling, D. R., Louis Smith, G., Keyes, D. F., Kato, S., Manalo-Smith, N. and Wong, T.: Toward Optimal Closure of the Earth's Top-of-Atmosphere Radiation Budget. J Cli, 22, 3, 748–766. doi: 10.1175/2008JCLI2637.1, 2009

Markus, T., Stroeve, J. C. and Miller, J.: Recent changes in Arctic sea ice melt onset, freezeup, and melt season length. J. Geophys. Res., 114, C12024. doi: 10.1029/2009JC005436, 2009

Martin, G. M., Bellouin, N., Collins, W. J., Culverwell, I. D., Halloran, P. R., Hardiman, S. C., Hinton, T. J., Jones, C. D., McDonald, R. E., McLaren, A. J., O'Connor, F. M., Roberts, M. J., Rodriguez, J. M., Woodward, S., Best, M. J., Brooks, M. E., Brown, A. R., Butchart, N., Dearden, C., Derbyshire, S. H., Dharssi, I., Doutriaux-Boucher, M., Edwards, J. M., Falloon, P. D., Gedney, N., Gray, L. J., Hewitt, H. T., Hobson, M., Huddleston, M. R., Hughes, J., Ineson, S., Ingram, W. J., James, P. M., Johns, T. C., Johnson, C. E., Jones, A., Jones, C. P., Joshi, M. M., Keen, A. B., Liddicoat, S., Lock, A. P., Maidens, A. V., Manners, J. C., Milton, S. F., Rae, J. G. L., Ridley, J. K., Sellar, A., Senior, C. A., Totterdell, I. J., Verhoef, A., Vidale, P. L. and Wiltshire, A., The HadGEM2 family of Met Office Unified Model climate configurations, Geosci. Model Dev., 4, 723-757, doi: https://doi.org/10.5194/gmd-4-723-2011, 2011

Maslanik, J., Stroeve, J. C., Fowler, C. and Emery, W.: Distribution and trends in Arctic sea ice age through spring 2011. Geophys. Res. Lett., 38, 47735. doi: 10.1029/2011GL047735, 2011

Massonnet, F., Fichefet, T., Goosse, H., Bitz, C. M., Philippon-Berthier, G., Holland, M. M. and Barriat, P.-Y.: Constraining projections of summer Arctic sea ice, The Cryosphere, 6, 1383–1394, doi: 10.5194/tc-6-1383-2012, 2012

Maykut, G. A. and McPhee, M. G., Solar heating of the Arctic mixed layer, J. Geophys. Res., 100, C12, 24,691-24,703, doi: 10.1029/95JC02554, 1995

McLaren, A. J., Banks, H. T., Durman, C. F., Gregory, J. M., Johns, T. C., Keen, A. B., Ridley, J. K., Roberts, M. J., Lipscomb, W. H., Connolley, W. M. and Laxon, S. W.: Evaluation of the sea ice simulation in a new coupled atmosphere-ocean climate model (HadGEM1). J. Geophys. Res., 111, C12014. doi: 10.1029/2005JC003033, 2006

McPhee, M. G., Kikuchi, T., Morison, J. H. and Stanton, T. P.: Ocean-to-ice heat flux at the North Pole environmental observatory, Geophys. Res. Lett., 30, 2274, doi:10.1029/2003GL018580, 2003

Notz, D.: How well must climate models agree with observations?. Philos T Roy Soc A, 373, 2052. doi: 10.1098/rsta.2014.0164, 2015

Perovich, D. K. and Elder, B., Estimates of ocean heat flux at SHEBA, Geophys. Res. Lett., 299, 9, 58-1 – 51-4, doi: 10.1029/2001GL014171, 2002

Perovich, D. K., Richter-Menge, J. A., Jones, K. F. and Light, B.: Sunlight, water, and ice: Extreme Arctic sea ice melt during the summer of 2007. Geophys. Res. Lett., 35, 11. doi: 10.1029/2008GL034007, 2008

Pithan, F., Medeiros, B. and Mauritsen, T.: Mixed-phase clouds cause climate model biases in Arctic wintertime temperature inversions, Clim. Dyn., 43, 289-303, doi:10.1007/s00382-013-1964-9, 2014

Raddatz, R. L., Papakyriakou, T. N., Else, B. G., Asplin, M. G., Candlish, L. M., Galley, R. J. and Barber, D. G.: Downwelling longwave radiation and atmospheric winter states in the western maritime Arctic. Int. J. Clim., 35, 9, 2339-2351. doi: 10.1002/joc.4149, 2014

Rayner, N. A., Parker, D. E., Horton, E. B., Folland, C. K., Alexander, L. V., Rowell, D. P., Kent, E. C. and Kaplan, A.: Global analyses of sea surface temperature, sea ice, and night marine air temperature since the late nineteenth century. J Geophys Res 108:4407. doi:10.1029/2002JD002670, 2003

Rothrock, D. A., Percival, D. B. and Wensnahan, M.: The decline in arctic sea ice thickness: Separating the spatial, annual, and interannual variability in a quarter century of submarine data. J. Geophys. Res., 113, C05003. doi: 10.1029/2007JC004252, 2008

Rutan, D. A., Kato, S., Doelling, D. R., Rose, F. G., Nguyen, L. T., Caldwell, T. E. and Loeb, N. G.: CERES Synoptic Product: Methodology and Validation of Surface Radiant Flux, J. Atmos. Ocean. Tech., 32(6), 1121-1143. http://dx.doi.org/10.1175/JTECH-D-14-00165.1, 2015

Schauer, U., Fahrbach, E., Osterhus, S. and Rohardt,, G.: Arctic warming through Fram Strait: Oceanic heat transport from 3 years of measurements, J. Geophys. Res. (Oceans), 109, C6, doi: 10.1029/2003JC001823, 2004.

Schweiger, A. J.., Lindsay, R. W., Zhang, J., Steele, M. and Stern, H.: Uncertainty in modeled arctic sea ice volume, J. Geophys. Res., doi:10.1029/2011JC007084, 2011

Semtner, A. J.: A Model for the Thermodynamic Growth of Sea Ice in Numerical Investigations of Climate. J. Phys. Oceanogr., 6, 3, 379–389. doi: 10.1175/1520-0485, 1976.

Serreze, M. C., Barrett, A. P., Slater, A. G., Woodgate, R. A., Aagaard, K., Lammers, R. B., Steele. M., Moritz, R., Meredith, M. and Lee, C. M.: The large-scale freshwater cycle of the Arctic, J. Geophys. Res., 111, C11010, doi:10.1029/2005JC003424, 2006

Shu, Q., Song, Z. and Qiao, F. (2015) Assessment of sea ice simulation in the CMIP5 models. The Cryosphere, 9, 399–409. doi: 10.5194/tc-9-399-2015

Stammerjohn, S., Massom, R., Rind, D. and Martinson, D: Regions of rapid sea ice change: An inter-hemispheric seasonal comparison, Geophys. Res. Lett., 39, 6. doi: 10.1029/2012GL050874, 212

Stramler, K., Del Genio, A. D. and Rossow, W. B.: Synoptically Driven Arctic Winter States. J. Clim., 24, 1747–1762. doi: 10.1175/2010JCLI3817.1, 2011

Steele, M. Zhang, J.; Ermold, W.: Mechanisms of summer Arctic Ocean warming, J. Geophys. Res. (Oceans), 115, C11, doi: 10.1029/2009JC005849 (2010)

Stroeve, J. C., Kattsov, V, Barrett, A., Serreze, M., Pavlova, T., Holland, M. M. and Meier, W. N.: Trends in Arctic sea ice extent from CMIP5, CMIP3 and observations. Geophys. Res. Lett., 39, doi: 10.1029/2012GL052676, 2012a.

Stroeve, J. C., Serreze, M. C., Holland, M. M., Kay, J. E., Maslanik, J., Barratt, A. P.: The Arctic's rapidly shrinking sea ice cover: a research synthesis, Clim. Ch., 110, 1005–1027, doi: https://doi.org/10.1007/s10584-011-0101-1, 2012b

Swart, N. C., Fyfe, J. C., Hawkins, E., Kay, J. E. and Jahn, A.: Influence of internal variability on Arctic sea ice trends, Nat. Clim. Ch., 5, 86–89, doi:10.1038/nclimate2483, 2015

Thorndike, A. S., Rothrock, D. A., Maykut, G. A. and Colony, R., The thickness distribution of sea ice, J. Geophys. Res., 80, 4501-4513, doi: 10.1029/JC080i033p04501, 1975

Tsamados, M., Feltham, D. L. and Wilchinsky, A. V., Impact of a new anisotropic rheology on simulations of Arctic sea ice, J. Geophys. Res. – Oceans, 118, 1, 91-107, doi: 10.1029/2012JC007990, 2013

Wang, M. and Overland, J. E.: A sea ice free summer Arctic within 30 years? Geophys. Res. Lett., ., 36, L07502, doi:10.1029/2009GL037820, 2009

Wang, X., Key, J., Kwok, R. and Zhang, J.: Comparison of Arctic Sea Ice Thickness from Satellites, Aircraft and PIOMAS data, Remote Sens., *8*(9), 713; doi:10.3390/rs8090713, 2016

Zhang, Y., Rossow, W. B., Lacis, A. A., Oinas, V., and Mishchenko, M. I.: Calculation of radiative fluxes from the surface to top of atmosphere based on ISCCP and other global data sets: Refinements of the radiative transfer model and the input data, J. Geophys. Res., 109, D19105, doi:10.1029/2003JD004457, 2004

Month	Downwelling SW	Downwelling LW	Ice thickness	Ice area	Melt onset occurrence	Total induced surface flux bias	Radiative flux bias	ISF residual	CERES-ERAI net radiation difference
Jan	0.0	-6.5	-4.3	2.7	0.0	-8.1	-1.6	3.3	-12.2
Feb	0.0	-4.8	-2.8	2.3	0.0	-5.3	-10.4	4.6	-12.5
Mar	0.1	-3.8	-2.0	2.0	0.0	-3.7	-10.5	5.9	-12.0
Apr	0.4	-4.4	-1.4	1.4	0.2	-4.2	-12.2	7.6	-9.7
May	2.1	-4.8	-0.6	0.0	0.1	-3.2	-3.7	0.5	-3.5
Jun	-8.3	7.4	0.0	1.7	11.4	12.2	27.8	-15.4	-4.2
Jul	-13.6	8.0	0.0	3.7	3.3	1.4	5.1	-3.9	-16.9
Aug	0.5	-3.3	-0.1	9.6	1.9	8.5	8.6	-0.0	-12.9
Sep	3.3	-7.1	-0.7	-0.7	0.0	-5.2	-0.2	-4.8	-2.4
Oct	0.9	-5.7	-4.2	-1.8	0.0	-10.8	-14.4	3.4	-4.6
Nov	0.0	-5.4	-8.3	-0.3	0.0	-14.0	-21.6	8.1	-11.7
Dec	0.0	-6.4	-6.4	2.4	0.0	-10.4	-14.9	4.1	-12.2

Table 1. Surface flux biases induced by model bias in 5 different variables in HadGEM2-ES (Wm^{-2}), with CERES used as reference dataset for the radiative components. Total ISF bias and total net radiative flux bias relative to CERES are shown for comparison, as well as their residual; the difference between net radiative flux bias as evaluated by CERES and ERAI is also shown. A positive number denotes a downwards flux, and vice versa.

Figure 1. The Arctic Ocean region used in the analysis.

1

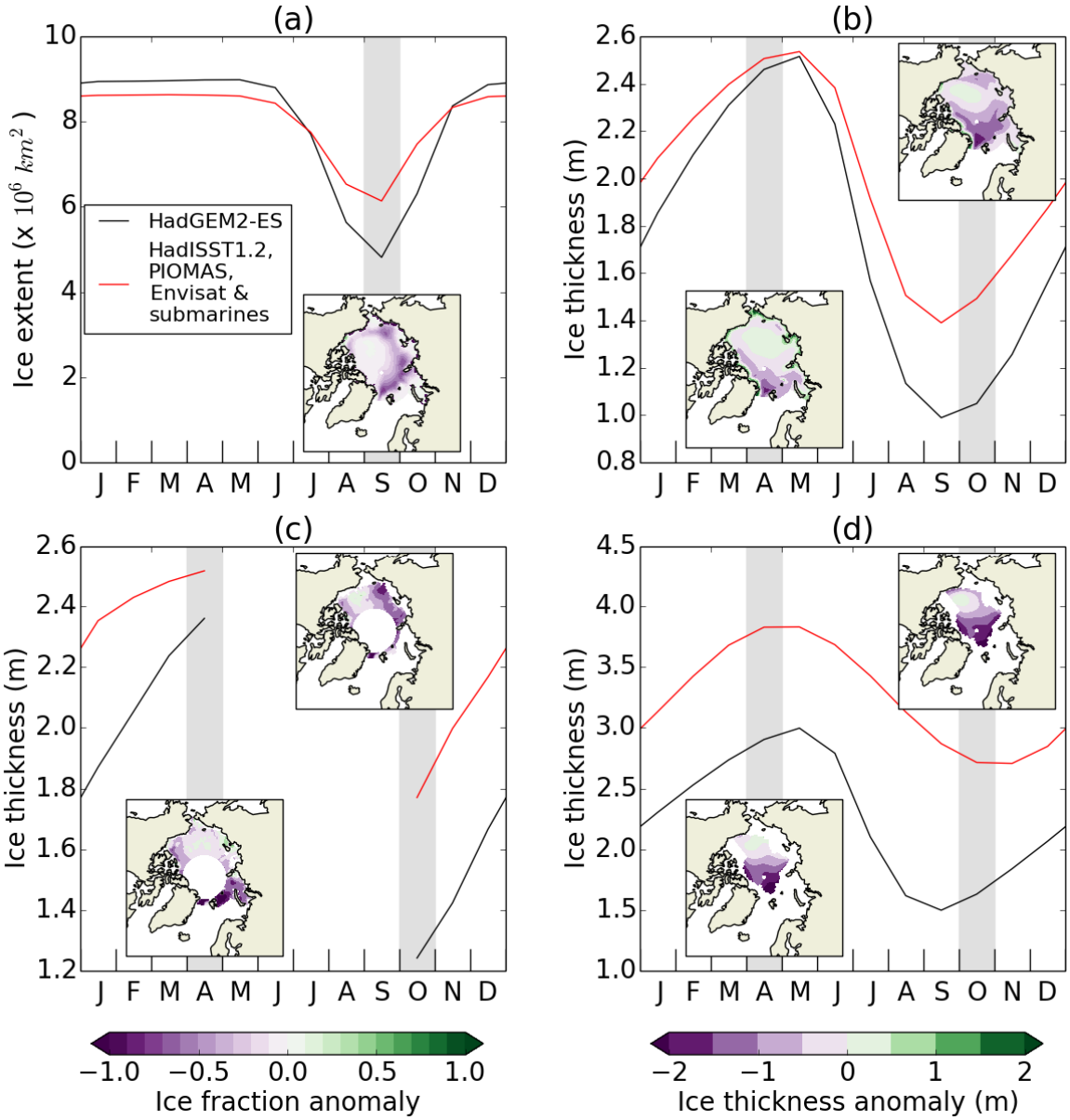

Figure 2. (a) HadGEM2-ES 1980-1999 mean Arctic Ocean ice extent, compared to HadISST1.2 1980-1999, with September ice fraction bias map; (b-d) HadGEM2-ES 1980-1999 ice thickness compared to (b) PIOMAS, (c) Envisat and (d) submarine datasets over respective regions of coverage, with April and October ice thickness bias maps. For each seasonal cycle plot, the model is in black and observations in red. In (c), data is not plotted from May-September due to the region of coverage being very small.

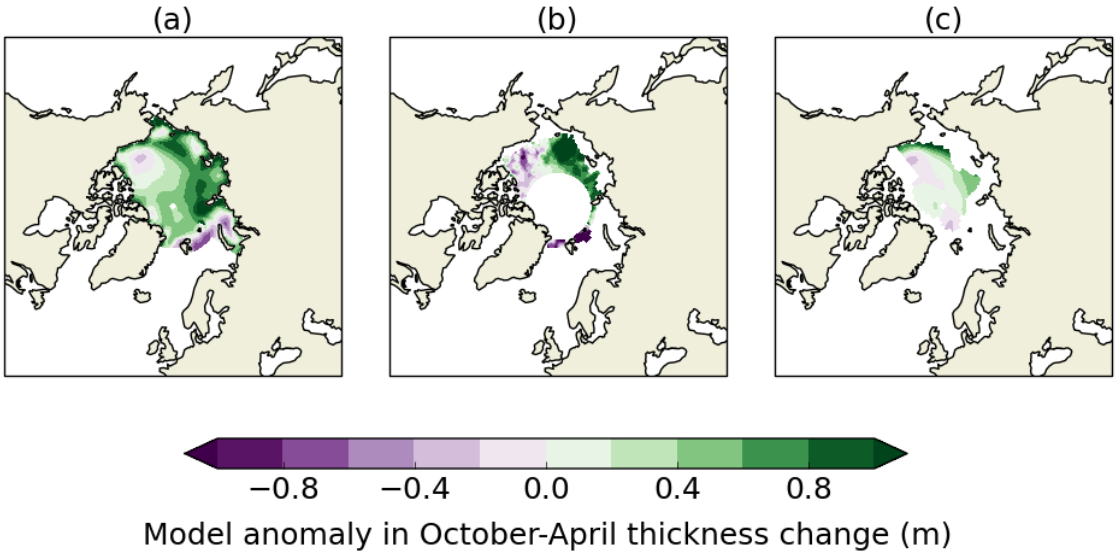

Figure 3. HadGEM2-ES 1980-1999 model bias in ice thickness change from October-April compared to (a) PIOMAS 1980-1999; (b) Envisat 1993-2000; (c) submarine regression analysis 1980-1999. Differences are taken as model-observation so that areas of green (purple) correspond to areas where the HadGEM2-ES model simulates too much (not enough) sea ice growth through the winter

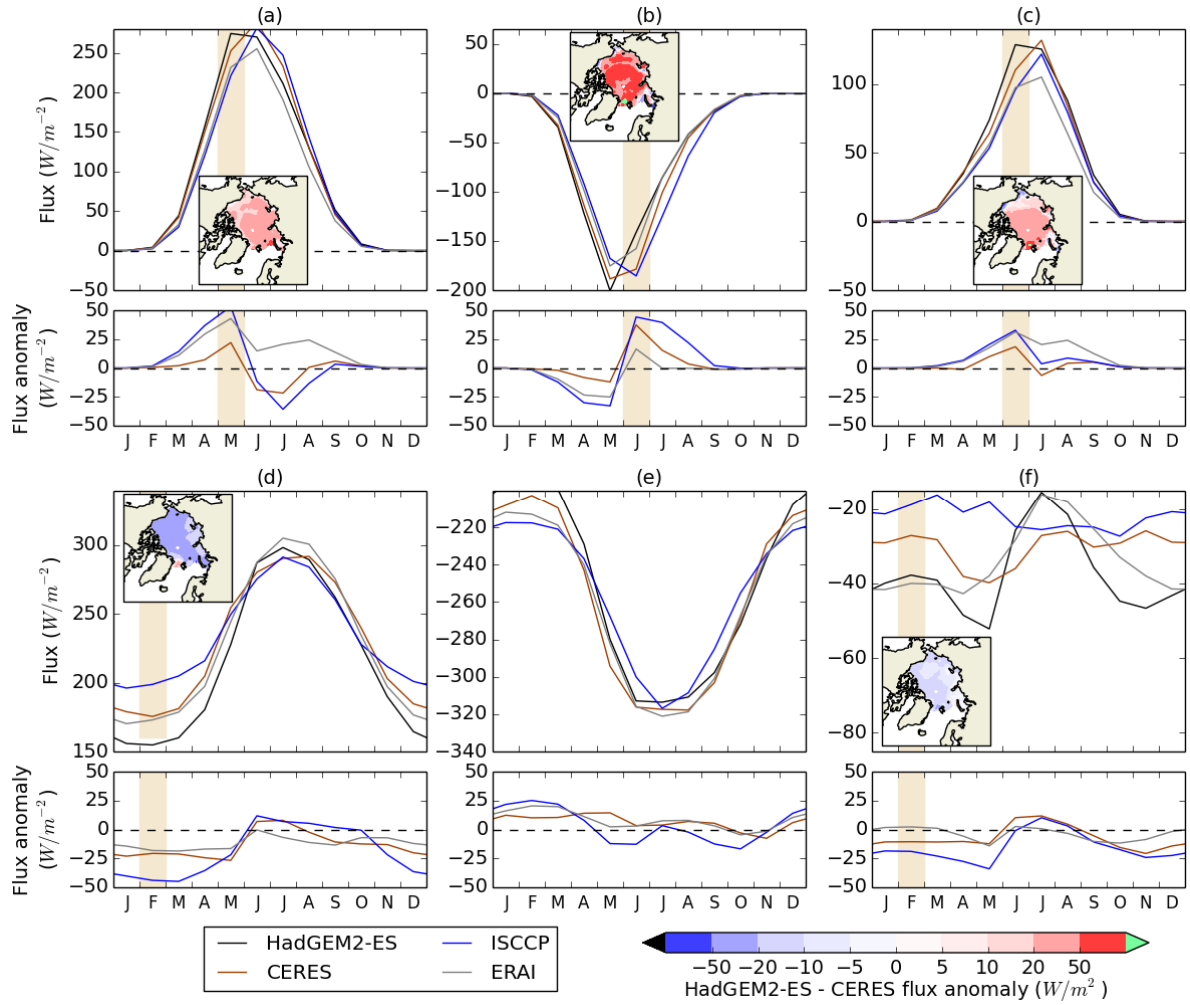

Figure 4. (a) Downwelling SW, (b) upwelling SW, (c) net down SW, (d) downwelling LW, (e) upwelling LW, (f) net down LW, for HadGEM2-ES 1980-1999 over the Arctic Ocean region, compared to CERES 2000-2013, ISCCP-D 1983-1999 and ERAI 1980-1999. For all fluxes, a positive number denotes a downward flux and vice versa. Maps of flux bias relative to CERES are shown for downwelling SW in May, upwelling and net down SW in June, and downwelling and net down LW in February.

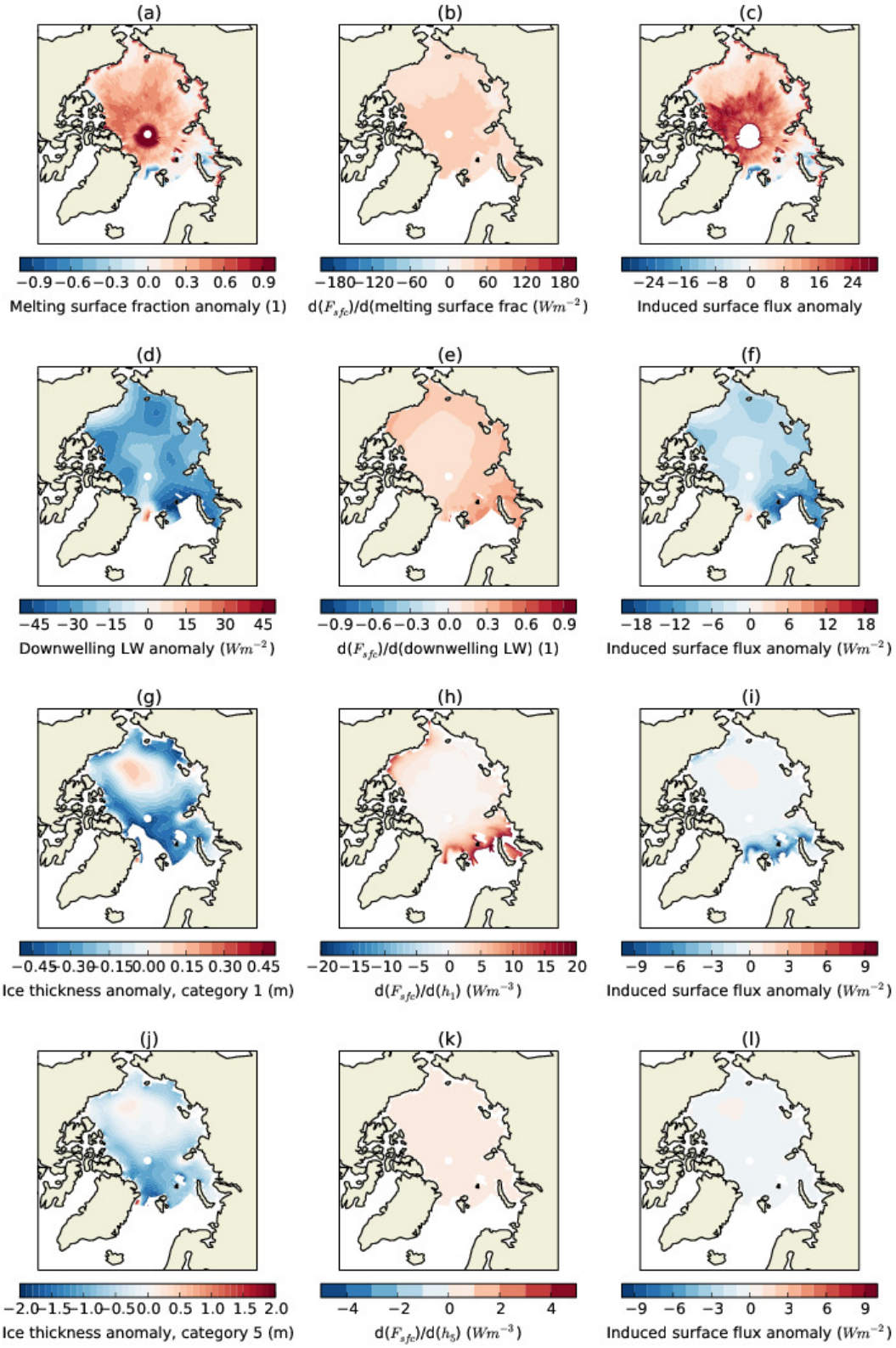

Figure 5. Demonstrating the calculation of fields of surface flux bias due to model bias in melting surface fraction (a-c), downwelling LW (d-f), category 1 ice thickness (g-i) and category 5 ice thickness (j-l). The left-hand column shows model bias in each variable; the middle column the local rate of dependence of surface flux on each variable as calculated above; the right column the induced surface flux bias, calculated as the product of these two fields.

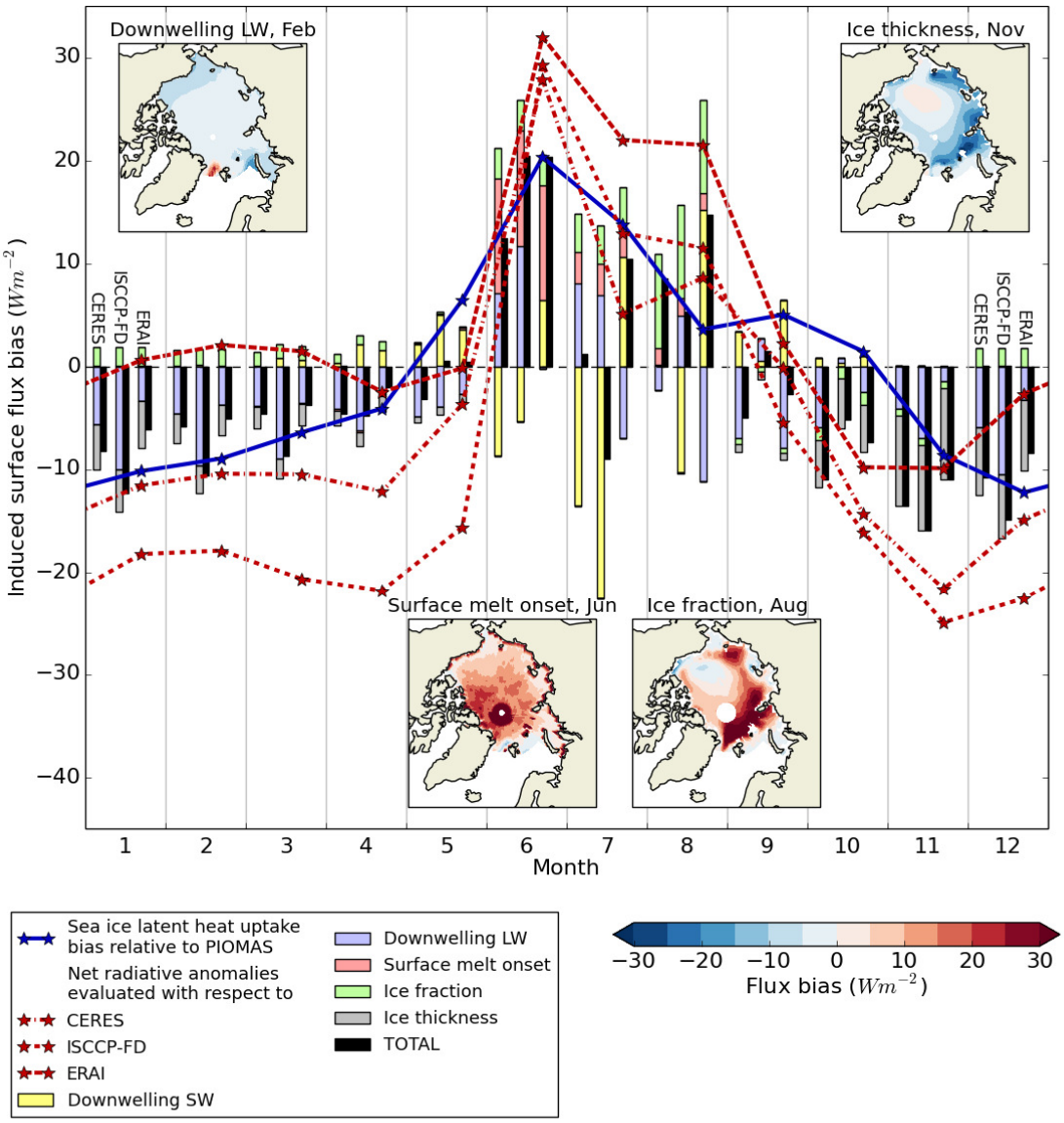

Figure 6. Surface flux bias induced by model biases in ice fraction, melt onset occurrence, ice thickness, downwelling SW and downwelling LW respectively, for the Arctic Ocean region in HadGEM2-ES, 1980-1999, as estimated by the simple models described in Section 2.3. For each month, induced surface flux biases are estimated using in turn CERES, ISCCP-FD and ERAI as radiation reference datasets, from left-right. Sea ice latent heat flux uptake bias relative to PIOMAS is indicated in black. Net radiative flux biases relative to CERES, ISCCP-FD and ERAI are indicated in brown. Spatial patterns of induced surface flux bias for four processes in key months, with CERES as reference dataset, are displayed beneath.

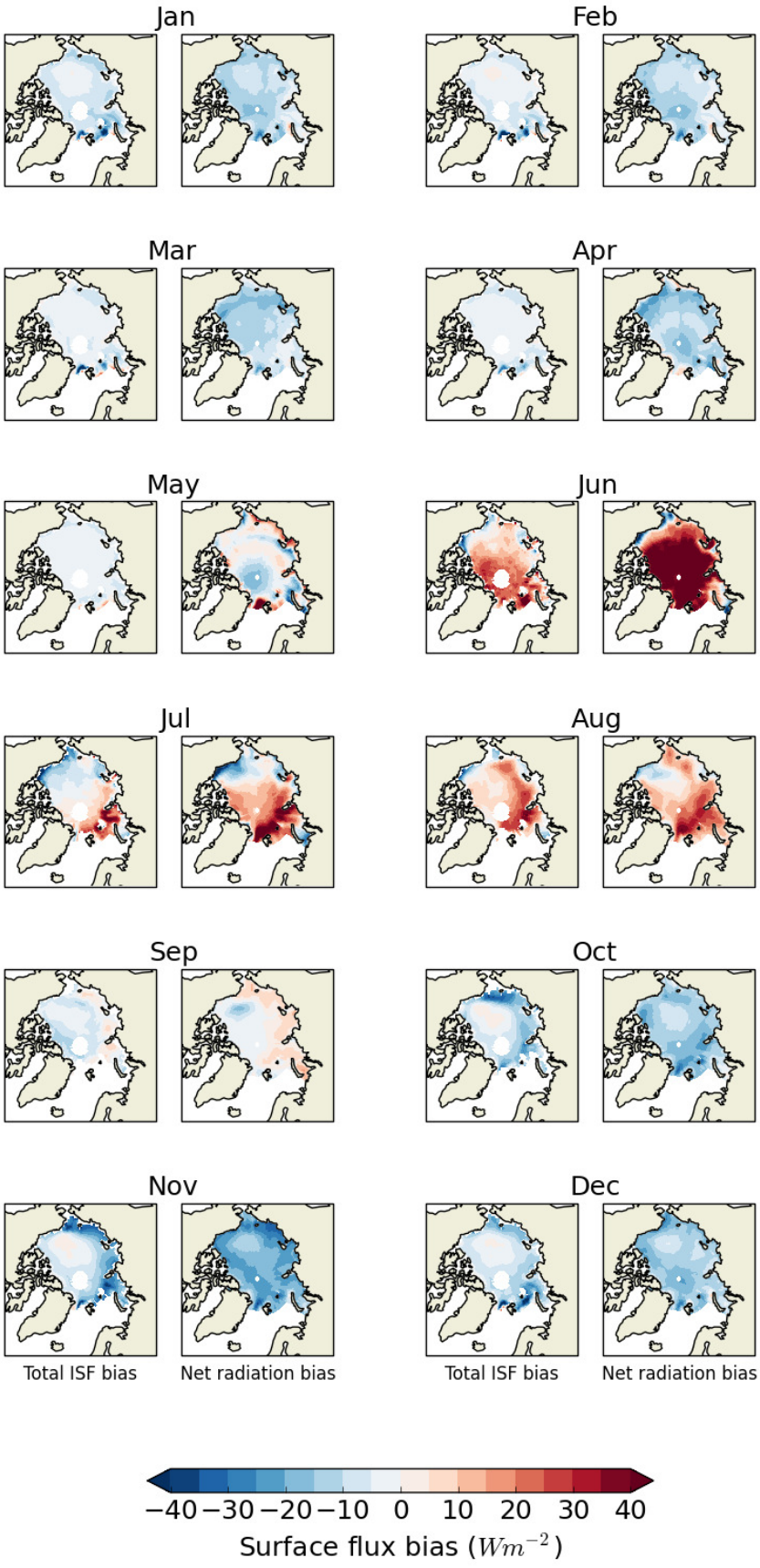

Figure 7. Comparing fields of total ISF bias to net radiation bias relative to CERES for each month of the year, for the four historical members of HadGEM2-ES, 1980-1999.

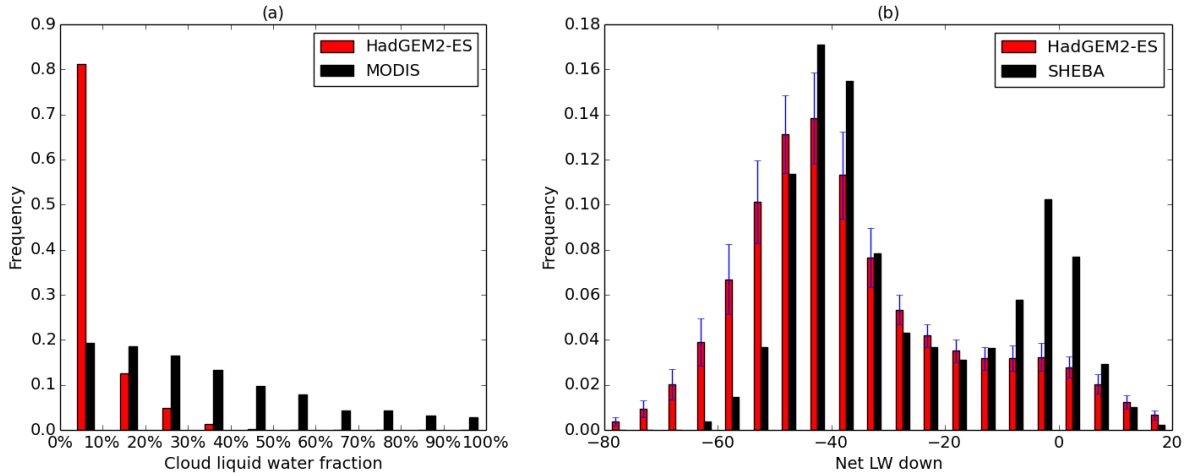

Figure 8. Frequency distributions of (a) October-April cloud liquid water percentage in HadGEM2-ES compared to MODIS observations, for the Arctic Ocean region; (b) December-February surface net downwelling LW in HadGEM2-ES in the SHEBA region, compared to the values observed at SHEBA.

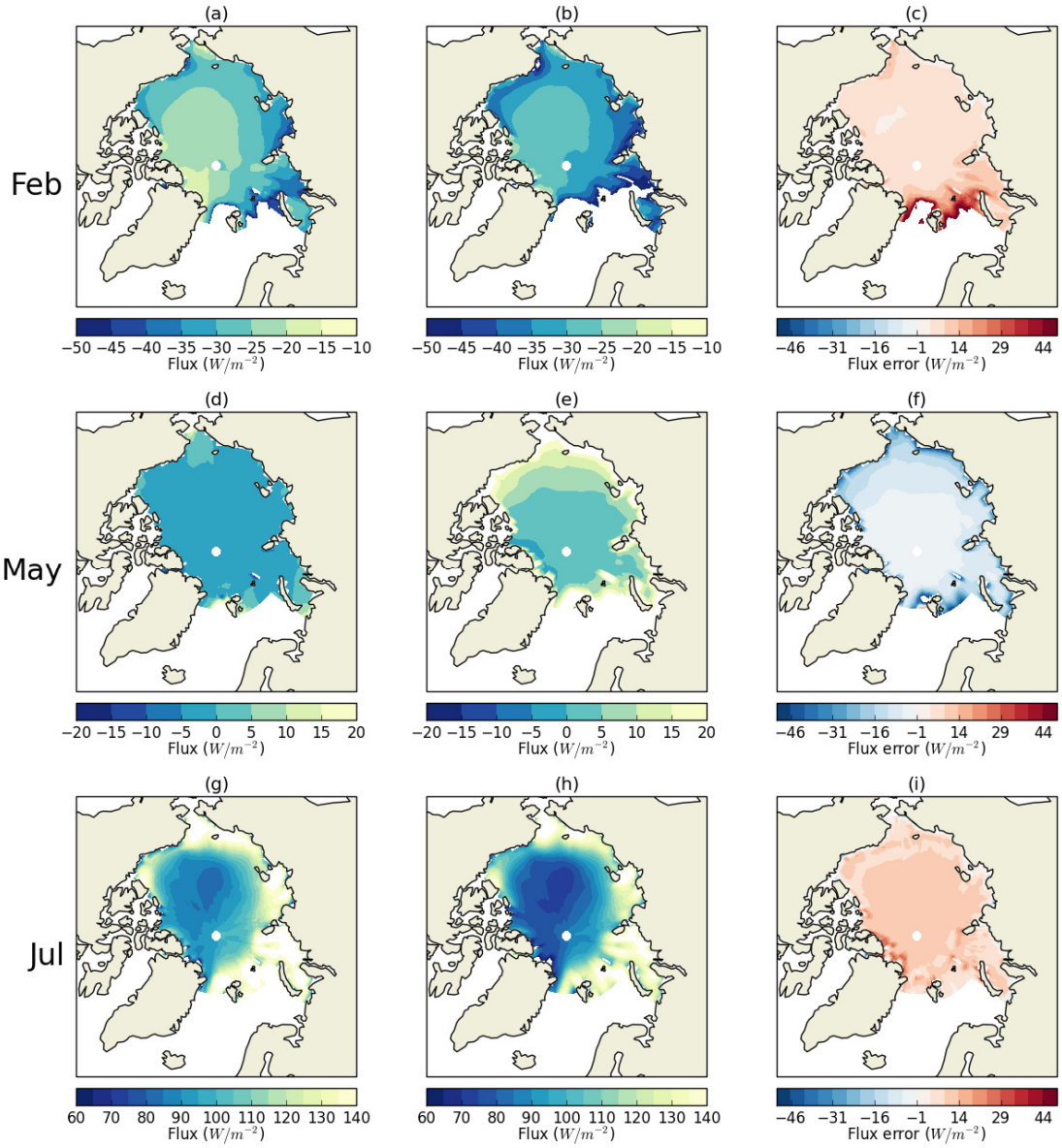

Figure A1. Illustrating approximated (left) and actual (centre) model net surface flux, as well as the approximation error (right), in (a-c) February; (d-f) May; (g-i) July, for the period 1980-1999 in the first historical run of HadGEM2-ES.